β decay and evolution of low-lying structure in Ge and As nuclei

Kosuke Nomura*

Department of Physics, Faculty of Science, University of Zagreb, HR-10000 Zagreb, Croatia

(Received 17 February 2022; revised 15 March 2022; accepted 23 March 2022; published 8 April 2022)

A simultaneous calculation for the shape evolution and the related spectroscopic properties of the low-lying states, and the β-decay properties in the even- and odd-mass Ge and As nuclei in the mass $A \approx 70$–80 region, within the framework of the nuclear density functional theory and the particle-core coupling scheme, is presented. The constrained self-consistent mean-field calculations using a universal energy density functional (EDF) and a pairing interaction determines the interacting-boson Hamiltonian for the even-even core nuclei, and the essential ingredients of the particle-boson interactions for the odd-nucleon systems, and of the Gamow-Teller and Fermi transition operators. A rapid structural evolution from γ-soft oblate to prolate shapes, as well as the spherical-oblate shape coexistence around the neutron subshell closure $N = 40$, is suggested to occur in the even-even Ge nuclei. The predicted low-energy spectra, electromagnetic transition rates, and β-decay $\log ft$ values are in a reasonable agreement with experiment. The predicted $\log ft$ values reflect the structures of the wave functions for the initial and final nuclei of β decay, which are, to a large extent, determined by the microscopic input provided by the underlying EDF calculation.

DOI: 10.1103/PhysRevC.105.044306

I. INTRODUCTION

β decay of the atomic nucleus is a weak-interaction process that converts protons into neutrons or vice versa, and is one of the important fundamental nuclear processes that not only helps to understand the structure of an individual nucleus, but is also essential for modeling astrophysical phenomena such as the nucleosynthesis of neutron-rich heavy elements. Experiments have been carried out at major radioactive-ion-beam facilities around the world, providing a wealth of new data on the β-decay half-lives of neutron-rich heavy nuclei [1–5]. From a theoretical point of view, calculation of the β decay properties should be sensitive to the nature of the wave functions of the initial and final nuclei, and hence serves as a benchmark of theoretical models. A number of theoretical investigations for the β decay have been made from various approaches such as the interacting boson and boson-fermion models (IBM and IBFM) [6–13], the quasiparticle random-phase approximations [14–21], and the nuclear shell model [22–25].

Precise measurements and theoretical investigations of the β-decay properties are also vital for determining matrix elements of double-β ($\beta\beta$) decay, a process in which two successive β decays occur between those nuclei with (A, Z) and $(A, Z \pm 2)$. Especially, the zero-neutrino mode of the $\beta\beta$ decay ($0\nu\beta\beta$) is not allowed in the standard model of elementary particles, and the observation of this process would greatly advance current understandings of the electroweak fundamental symmetries [26].

The nuclei in the germanium (Ge) region around the neutron number $N = 40$ is among the challenging regions of the nuclear chart, and has been of great interests for recent theoretical [27–32] and experimental studies [33–38]. Their low-lying states are characterized by a rich variety of nuclear structure phenomena, represented by a rapid shape evolution from one nucleus to another, which includes the emergence of the neutron $N = 40$ subshell closure around ^{72}Ge, the competition between multiple intrinsic shapes in the vicinity of the ground state within a single nucleus, i.e., shape coexistence [35,39], and the triaxial deformation around ^{76,78}Ge [33,36]. The nucleus ^{76}Ge is of special importance, since it is a candidate nucleus as the $0\nu\beta\beta$ decay emitter, and its odd-odd neighbor ^{76}As is considered a virtual intermediate state of the $\beta\beta$ decay.

In this paper, the β-decay rates and the evolution of low-lying collective structure of the even-A and odd-A Ge and the neighboring arsenic (As) isotopes in the $A \approx 70$–80 region is investigated within a framework of the nuclear density functional theory and the particle-core coupling scheme. In this method, first the potential energy surfaces with the triaxial quadrupole shape degrees of freedom for the even-even nuclei are computed by means of the constrained self-consistent mean-field (SCMF) [40] calculations based on a universal energy density functional (EDF) and a pairing interaction. The low-lying structure of the even-even core nucleus is described by the IBM, with the Hamiltonian determined by mapping the SCMF energy surface onto the expectation value of the Hamiltonian [41]. The particle-core coupling for the odd-A and odd-odd systems is modelled within the frameworks of the IBFM [42,43] and the interacting boson-fermion-fermion models (IBFFM) [43,44], respectively. The essential ingredients of the particle-boson interaction terms, and of the

*knomura@phy.hr

Gamow-Teller and Fermi transition operators are determined by the same SCMF calculations. This theoretical procedure allows for a consistent calculation of nuclear β decay and low-lying structure in a computationally feasible way, and has been used for studies of the β decays of the odd-A [11] and even-A [12] Xe, Cs, Ba, and La regions with mass $A \approx 130$, using as a microscopic input the Gogny-type EDF [45].

The paper is organized as follows. In Sec. II the theoretical framework, including the SCMF method, the procedure to construct the particle-core Hamiltonian, and the electromagnetic, Gamow-Teller, and Fermi transition operators, is described. In Sec. III, the calculated deformation energy surfaces and spectroscopic properties of the low-lying states of the even-even Ge nuclei, and the possible shape coexistence in ^{72}Ge are discussed. The spectroscopic results for the odd-mass Ge and As, and the odd-odd As nuclei are shown in Secs. IV and V, respectively. In Sec. VI the ft values for the β decays between the odd-mass and between the odd-odd nuclei are shown. Section VII summarizes the main results.

II. THEORETICAL FRAMEWORK

A. Self-consistent mean-field calculations

As the first step, the constrained SCMF calculations for the even-even $^{66-78}$Ge nuclei are performed within the relativistic Hartree-Bogoliubov (RHB) framework [46–48] with the density-dependent point-coupling (DD-PC1) [49] functional for the particle-hole channel, and a separable pairing force of finite range [50] for the particle-particle channel. The constraints imposed in the SCMF calculations are on the mass quadrupole moments, which are related to the polar deformation variables β and γ [51]. The constrained calculations produce the (β, γ)-deformation energy surfaces.

B. Particle-core Hamiltonian

To compute the spectroscopic observables such as excitation spectra and transition rates, it is required to go beyond the static SCMF approximation, including the dynamical correlations arising from the restoration of broken symmetries and fluctuations in the collective coordinates [40].

The spectroscopic calculation is here carried out in terms of the IBM. In the following, the neutron-proton IBM (IBM-2) [52] is used, because it is suitable to treat β decay, in which both proton and neutron degrees of freedom should be explicitly considered. The IBM-2 consists of the neutron and proton monopole (s_ν and s_π), and quadrupole (d_ν and d_π) bosons. From a microscopic point of view [52,53], the s_ν (s_π) and d_ν (d_π) bosons are associated with the collective S_ν (S_π) and D_ν (D_π) pairs of valence neutrons (protons) with angular momenta $J = 0^+$ and $J = 2^+$, respectively. Here, the neutron (or proton) major oscillator shell N(or Z) = 28–50 is taken as the model space of the neutron (or proton) boson system. Hence for the $^{66-78}$Ge nuclei considered in this study, the number of the neutron bosons, N_ν, varies within the range $2 \leqslant N_\nu \leqslant 5$, while the number of the proton bosons is fixed, $N_\pi = 2$.

To deal with the even-even, odd-mass, and odd-odd nuclei simultaneously, both the collective (bosonic) and single-particle degrees of freedom are treated on the footing, within the neutron-proton IBFFM (IBFFM-2). The Hamiltonian of the IBFFM-2 is given by

$$\hat{H} = \hat{H}_{\rm B} + \hat{H}_{\rm F}^{\nu} + \hat{H}_{\rm F}^{\pi} + \hat{V}_{\rm BF}^{\nu} + \hat{V}_{\rm BF}^{\pi} + \hat{V}_{\nu\pi}, \tag{1}$$

where $\hat{H}_{\rm B}$ is the IBM-2 Hamiltonian representing the bosonic even-even core, $\hat{H}_{\rm F}^{\nu}$ ($\hat{H}_{\rm F}^{\pi}$) is the single-neutron (proton) Hamiltonian, $\hat{V}_{\rm BF}^{\nu}$ ($\hat{V}_{\rm BF}^{\pi}$) represents the interaction between the odd neutron (proton) and the even-even IBM-2 core, and the last term $\hat{V}_{\nu\pi}$ is the residual neutron-proton interaction.

For the IBM-2 Hamiltonian the following form is employed:

$$\hat{H}_{\rm B} = \epsilon_d \left(\hat{n}_{d_\nu} + \hat{n}_{d_\pi}\right) + \kappa \hat{Q}_\nu \hat{Q}_\pi + \kappa' \hat{L}\hat{L}, \tag{2}$$

where in the first term, $\hat{n}_{d_\rho} = d_\rho^\dagger \tilde{d}_\rho$ ($\rho = \nu$ or π) is the d-boson number operator with ϵ_d the single d-boson energy relative to the s-boson one, and $\tilde{d}_{\rho\mu} = (-1)^\mu d_{\rho-\mu}$. The second term stands for the quadrupole-quadrupole interaction between neutron and proton boson systems with strength κ, and $\hat{Q}_\rho = d_\rho^\dagger s_\rho + s_\rho^\dagger \tilde{d}_\rho + \chi_\rho (d_\rho^\dagger \times \tilde{d}_\rho)^{(2)}$ is the bosonic quadrupole operator, with the parameter χ_ρ. The last term in Eq. (2) is a rotational term with strength κ', where $\hat{L} = \sqrt{10}\sum_\rho (d_\rho^\dagger \times \tilde{d}_\rho)^{(1)}$ is the bosonic angular momentum operator.

The single-nucleon Hamiltonian $\hat{H}_{\rm F}^{\rho}$ takes the form

$$\hat{H}_{\rm F}^{\rho} = -\sum_{j_\rho} \epsilon_{j_\rho} \sqrt{2j_\rho + 1} \left(a_{j_\rho}^\dagger \times \tilde{a}_{j_\rho}\right)^{(0)} \equiv \sum_{j_\rho} \epsilon_{j_\rho} \hat{n}_{j_\rho}, \tag{3}$$

where ϵ_{j_ρ} stands for the single-particle energy of the odd neutron ($\rho = \nu$) or proton ($\rho = \pi$) orbital j_ρ. $a_{j_\rho}^{(\dagger)}$ represents particle annihilation (creation) operator, with $\tilde{a}_{j_\rho}$ defined by $\tilde{a}_{j_\rho m_\rho} = (-1)^{j_\rho - m_\rho} a_{j_\rho - m_\rho}$. On the right-hand side of Eq. (3), $\hat{n}_{j_\rho}$ stands for the number operator for the odd particle. For the fermion configuration space, the normal-parity orbitals $2p_{1/2}$, $2p_{3/2}$, and $1f_{5/2}$, for both neutron and proton are taken.

The boson-fermion interaction $\hat{V}_{\rm BF}^{\rho}$ here has a specific form [43]:

$$\hat{V}_{\rm BF}^{\rho} = \Gamma_\rho \hat{V}_{\rm dyn}^{\rho} + \Lambda_\rho \hat{V}_{\rm exc}^{\rho} + A_\rho \hat{V}_{\rm mon}^{\rho}. \tag{4}$$

The first, second, and third terms are dynamical quadrupole, exchange, and monopole interactions, respectively. By following the microscopic considerations with the generalized seniority scheme [43,54], these are given as

$$\hat{V}_{\rm dyn}^{\rho} = \sum_{j_\rho j'_\rho} \gamma_{j_\rho j'_\rho} \left(a_{j_\rho}^\dagger \times \tilde{a}_{j'_\rho}\right)^{(2)} \hat{Q}_{\rho'}, \tag{5}$$

$$\hat{V}_{\rm exc}^{\rho} = -(s_{\rho'}^\dagger \times \tilde{d}_{\rho'})^{(2)} \sum_{j_\rho j'_\rho j''_\rho} \sqrt{\frac{10}{N_\rho (2j_\rho + 1)}} \beta_{j_\rho j'_\rho} \beta_{j''_\rho j_\rho} : \left(\left(d_\rho^\dagger \times \tilde{a}_{j''_\rho}\right)^{(j_\rho)} \times \left(a_{j'_\rho}^\dagger \times \tilde{s}_\rho\right)^{(j'_\rho)}\right)^{(2)} : + ({\rm H.c.}), \tag{6}$$

$$\hat{V}_{\rm mon}^{\rho} = \hat{n}_{d_\rho} \hat{n}_{j_\rho}, \tag{7}$$

where the factors $\gamma_{j_\rho j'_\rho} = (u_{j_\rho} u_{j'_\rho} - v_{j_\rho} v_{j'_\rho}) Q_{j_\rho j'_\rho}$, and $\beta_{j_\rho j'_\rho} = (u_{j_\rho} v_{j'_\rho} + v_{j_\rho} u_{j'_\rho}) Q_{j_\rho j'_\rho}$ with $Q_{j_\rho j'_\rho} = \langle \ell_\rho \tfrac{1}{2} j_\rho \| Y^{(2)} \| \ell'_\rho \tfrac{1}{2} j'_\rho \rangle$ matrix element of the fermion quadrupole operator in the single-particle basis. $\hat{Q}_{\rho'}$ in Eq. (5) is the same boson

TABLE I. Derived strength parameters for the IBM-2 Hamiltonian $\hat{H}_{\rm B}$ for the even-even $^{66-78}$Ge nuclei.

Nucleus	ϵ_d (MeV)	κ (MeV)	χ_ν	χ_π	κ' (MeV)
^{66}Ge	0.061	−0.680	−0.07	0.30	0.015
^{68}Ge	0.091	−0.540	0.20	0.30	0.051
^{70}Ge	0.535	−0.350	0.80	0.50	0.069
^{72}Ge	0.747	−0.180	0.30	0.30	0.050
^{74}Ge	0.950	−0.315	0.30	0.30	0.000
^{76}Ge	0.600	−0.380	−0.90	−0.50	0.000
^{78}Ge	0.620	−0.620	−1.12	−0.87	0.000

quadrupole operator as in the boson Hamiltonian (2). The notation : $(\cdots)$: in Eq. (6) stands for normal ordering. Within the above formalism, the dynamical and exchange terms are dominated by the interactions between unlike particles, while the monopole term by like particle ones. In addition, the single-particle energy ϵ_{j_ρ} is replaced with the quasiparticle energy $\tilde{\epsilon}_{j_\rho}$.

For the residual neutron-proton interaction $\hat{V}_{\nu\pi}$ in Eq. (1), the following form [55] is adopted:

$$\hat{V}_{\nu\pi} = 4\pi\, v_{\rm d}\delta(\boldsymbol{r})\delta(\boldsymbol{r}_\nu - r_0)\delta(\boldsymbol{r}_\pi - r_0) + v_{\rm t}\left[\frac{3(\boldsymbol{\sigma}_\nu\mathbf{r})(\boldsymbol{\sigma}_\pi\mathbf{r})}{r^2} - \boldsymbol{\sigma}_\nu\boldsymbol{\sigma}_\pi\right], \tag{8}$$

where the first and second terms are δ and tensor interactions with strength parameters $v_{\rm d}$, and $v_{\rm t}$, respectively. Note that $\boldsymbol{r} = \boldsymbol{r}_\nu - \boldsymbol{r}_\pi$ and $r_0 = 1.2A^{1/3}$ fm.

C. Procedure to build the Hamiltonian

To construct the IBFFM-2 Hamiltonian (1), first the IBM-2 Hamiltonian for the even-even core is determined. The parameters ϵ_d, κ, χ_ν, and χ_π are determined by mapping the SCMF energy surface onto the expectation value of the Hamiltonian in the boson coherent state [56,57], so that the SCMF and IBM energy surfaces becomes similar to each other within the excitation energy of a few MeV with respect to the global minimum (see Refs. [41,58], for details). The remaining parameter κ' is fixed separately, in such a way [59] that the cranking moment of inertia calculated in the intrinsic frame of the boson system at the global minimum becomes equal to the Inglis-Belyaev [60,61] value calculated by the RHB method. The derived IBM-2 parameters are listed in Table I.

Second, for each odd-mass nucleus the quasiparticle energies $\tilde{\epsilon}_{j_\rho}$ and occupation probabilities $v^2_{j_\rho}$ of the odd nucleons are calculated by the RHB method constrained to zero deformation $\beta = 0$. These quantities are then used for the single-nucleon Hamiltonian $\hat{H}^\rho_{\rm F}$ (3) and the boson-fermion interactions $\hat{V}^\rho_{\rm BF}$ (4)–(6). Here, the fixed values of the strength parameters are adopted: $\Gamma_\nu = 0.3$ MeV, $\Lambda_\nu = 0.8$ MeV, and $A_\nu = -0.5$ MeV for the odd-N Ge nuclei, and $\Gamma_\pi = 0.3$ MeV, $\Lambda_\pi = 0.3$ MeV, and $A_\pi = 0$ MeV for the odd-Z As. These values are determined so as to reasonably reproduce the experimental data on the low-energy negative-parity excitation spectra for the odd-mass nuclei.

Third, the same strength parameters $\{\Gamma_\rho, \Lambda_\rho, A_\rho\}$ as the ones employed for the neighboring odd-mass nuclei are used for the IBFFM-2 calculation on the odd-odd As ones. The quasiparticle energies and occupation probabilities are newly calculated. Finally, the fixed values of the strength parameters for the interaction $\hat{V}_{\nu\pi}$, $v_{\rm d} = 0.8$ MeV and $v_{\rm t} = 0.02$ MeV, are determined so that an overall reasonable agreement with the observed low-lying positive-parity states of the odd-odd As nuclei is obtained.

TABLE II. Even-even Ge core, neighboring odd-N Ge, odd-Z As, and odd-odd As nuclei considered in the present study.

Core	odd-N	odd-Z	odd-odd
$^{66}_{32}$Ge$_{34}$	$^{67}_{32}$Ge$_{35}$	$^{67}_{33}$As$_{34}$	$^{68}_{33}$As$_{35}$
$^{68}_{32}$Ge$_{36}$	$^{69}_{32}$Ge$_{37}$	$^{69}_{33}$As$_{36}$	$^{70}_{33}$As$_{37}$
$^{70}_{32}$Ge$_{38}$	$^{71}_{32}$Ge$_{39}$	$^{71}_{33}$As$_{38}$	$^{72}_{33}$As$_{39}$
$^{72}_{32}$Ge$_{40}$		$^{73}_{33}$As$_{40}$	
$^{74}_{32}$Ge$_{42}$	$^{73}_{32}$Ge$_{41}$	$^{75}_{33}$As$_{42}$	$^{74}_{33}$As$_{41}$
$^{76}_{32}$Ge$_{44}$	$^{75}_{32}$Ge$_{43}$	$^{77}_{33}$As$_{44}$	$^{76}_{33}$As$_{43}$
$^{78}_{32}$Ge$_{46}$	$^{77}_{32}$Ge$_{45}$	$^{79}_{33}$As$_{46}$	$^{78}_{33}$As$_{45}$

Table II summarizes the even-even Ge core nuclei, and the neighboring odd-N Ge, odd-Z As, and odd-odd As nuclei considered in the present calculation. The ϵ_{j_ρ}, $\tilde{\epsilon}_{j_\rho}$, and $v^2_{j_\rho}$ values of the odd nucleons, obtained from the spherical RHB calculations, are shown in Fig. 1.

D. Electromagnetic transition operators

The $E2$ operator $\hat{T}^{(E2)}$ in the IBFM-2 and IBFFM-2 takes the form [43]

$$\hat{T}^{(E2)} = \hat{T}^{(E2)}_{\rm B} + \hat{T}^{(E2)}_{\rm F}, \tag{9}$$

where the first and second terms are the boson and fermion parts, given respectively as

$$\hat{T}^{(E2)}_{\rm B} = \sum_{\rho=\nu,\pi} e^{\rm B}_\rho \hat{Q}_\rho, \tag{10}$$

and

$$\hat{T}^{(E2)}_{\rm F} = -\frac{1}{\sqrt{5}}\sum_{\rho=\nu,\pi}\sum_{j_\rho j'_\rho}\left(u_{j_\rho}u_{j'_\rho} - v_{j_\rho}v_{j'_\rho}\right) \times \left\langle \ell_\rho \tfrac{1}{2} j_\rho \middle\| e^{\rm F}_\rho r^2 Y^{(2)} \middle\| \ell'_\rho \tfrac{1}{2} j'_\rho \right\rangle \left(a^\dagger_{j_\rho} \times \tilde{a}_{j'_\rho}\right)^{(2)}. \tag{11}$$

The fixed values for the boson effective charges $e^{\rm B}_\nu = e^{\rm B}_\pi = 0.0577$ eb are chosen so that the experimental $B(E2; 2^+_1 \to 0^+_1)$ value for the well-deformed even-even core nucleus ^{72}Ge is reproduced. The neutron and proton effective charges $e^{\rm F}_\nu = 0.5$ eb $e^{\rm F}_\pi = 1.5$ eb are adopted from the earlier IBFFM-2 calculation on the odd-odd Cs nuclei [62]. The $M1$ transition operator $\hat{T}^{(\rm M1)}$ reads

$$\hat{T}^{(M1)} = \sqrt{\frac{3}{4\pi}}\sum_{\rho=\nu,\pi}\left[g^{\rm B}_\rho \hat{L}_\rho - \frac{1}{\sqrt{3}}\sum_{j_\rho j'_\rho}\left(u_{j_\rho}u_{j'_\rho} + v_{j_\rho}v_{j'_\rho}\right) \times \left\langle j_\rho \middle\| g^\rho_l \mathbf{l} + g^\rho_s \mathbf{s} \middle\| j'_\rho \right\rangle \left(a^\dagger_{j_\rho} \times \tilde{a}_{j'_\rho}\right)^{(1)} \right]. \tag{12}$$

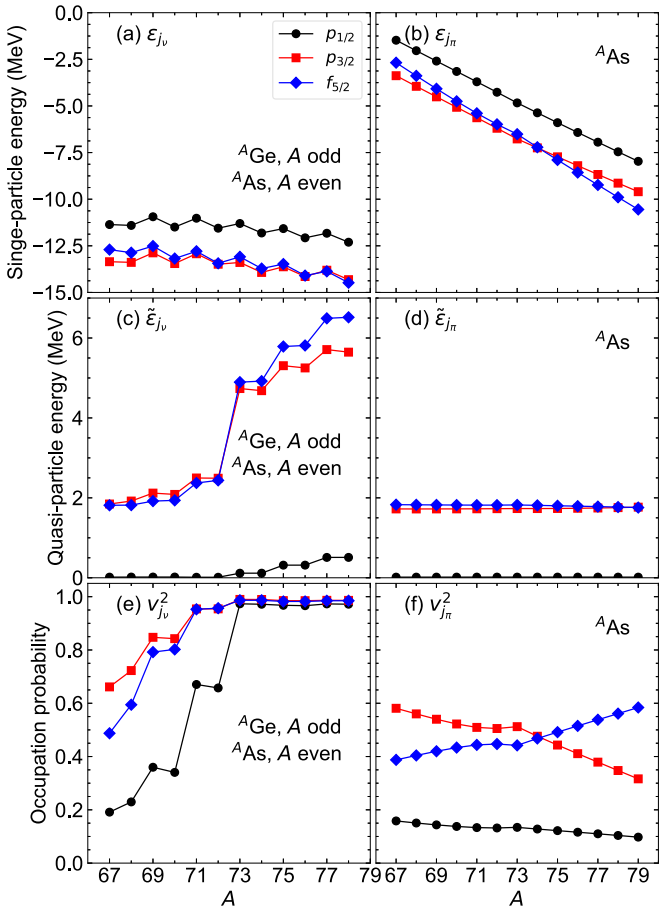

FIG. 1. The adopted spherical single-particle energies ϵ_{j_ρ} (a), (b), quasiparticle energies $\tilde{\epsilon}_{j_\rho}$ (c), (d), and occupation probabilities $v^2_{j_\rho}$ (e), (f) for the $2p_{1/2}$, $2p_{3/2}$, and $1f_{5/2}$ orbitals for (left column) the odd neutron in the odd-A Ge and even-A As, and (right column) the odd proton in the odd-A and even-A As nuclei, calculated by the spherical RHB method.

The empirical g factors for the neutron and proton bosons, $g^{\rm B}_\nu = 0\,\mu_N$ and $g^{\rm B}_\pi = 1.0\,\mu_N$, respectively, are adopted. For the neutron (or proton) g factors, the standard Schmidt values $g^\nu_l = 0\,\mu_N$ and $g^\nu_s = -3.82\,\mu_N$ ($g^\pi_l = 1.0\,\mu_N$ and $g^\pi_s = 5.58\,\mu_N$) are used with g^ρ_s quenched by 30% with respect to the free value.

E. Gamow-Teller and Fermi transition operators

The Gamow-Teller $\hat{T}^{\rm GT}$ and Fermi $\hat{T}^{\rm F}$ transition operators have the forms

$$\hat{T}^{\rm GT} = \sum_{j_\nu j_\pi} \eta^{\rm GT}_{j_\nu j_\pi} \left(\hat{P}_{j_\nu} \times \hat{P}_{j_\pi}\right)^{(1)}, \tag{13}$$

$$\hat{T}^{\rm F} = \sum_{j_\nu j_\pi} \eta^{\rm F}_{j_\nu j_\pi} \left(\hat{P}_{j_\nu} \times \hat{P}_{j_\pi}\right)^{(0)}, \tag{14}$$

respectively, with the coefficients

$$\eta^{\rm GT}_{j_\nu j_\pi} = -\frac{1}{\sqrt{3}} \left\langle \ell_\nu \tfrac{1}{2} j_\nu \middle\| \boldsymbol{\sigma} \middle\| \ell_\pi \tfrac{1}{2} j_\pi \right\rangle \delta_{\ell_\nu \ell_\pi}, \tag{15}$$

$$\eta^{\rm F}_{j_\nu j_\pi} = -\sqrt{2j_\nu + 1}\,\delta_{j_\nu j_\pi}. \tag{16}$$

$\hat{P}_{j_\rho}$ in Eqs. (13) and (14) is here identified as one of the one-particle creation operators

$$A^\dagger_{j_\rho m_\rho} = \zeta_{j_\rho} a^\dagger_{j_\rho m_\rho} + \sum_{j'_\rho} \zeta_{j_\rho j'_\rho} s^\dagger_\rho \left(\tilde{d}_\rho \times a^\dagger_{j'_\rho}\right)^{(j_\rho)}_{m_\rho}, \tag{17a}$$

$$B^\dagger_{j_\rho m_\rho} = \theta_{j_\rho} s^\dagger_\rho \tilde{a}_{j_\rho m_\rho} + \sum_{j'_\rho} \theta_{j_\rho j'_\rho} \left(d^\dagger_\rho \times \tilde{a}_{j'_\rho}\right)^{(j_\rho)}_{m_\rho}, \tag{17b}$$

and the annihilation operators

$$\tilde{A}_{j_\rho m_\rho} = (-1)^{j_\rho - m_\rho} A_{j_\rho - m_\rho}, \tag{17c}$$

$$\tilde{B}_{j_\rho m_\rho} = (-1)^{j_\rho - m_\rho} B_{j_\rho - m_\rho}. \tag{17d}$$

Note that the operators in Eqs. (17a) and (17c) conserve the boson number, whereas the ones in Eqs. (17b) and (17d) do not. The $\hat{T}^{\rm GT}$ and $\hat{T}^{\rm F}$ operators are formed as a combination of two of the operators in (17a)–(17d), depending on the type of the β decay under study (i.e., β^+ or β^-) and on the particle or hole nature of bosons in the even-even IBM-2 core. It is also noted that the expressions in Eqs. (17a)–(17d) are of simplified forms of the most general one-particle transfer operators in the IBFM-2 [43].

Within the generalized seniority scheme, the coefficients ζ_j, $\zeta_{jj'}$, θ_j, and $\theta_{jj'}$ in Eqs. (17a) and (17b) can be given by [63]

$$\zeta_{j_\rho} = u_{j_\rho} \frac{1}{K'_{j_\rho}}, \tag{18a}$$

$$\zeta_{j_\rho j'_\rho} = -v_{j_\rho} \beta_{j'_\rho j_\rho} \sqrt{\frac{10}{N_\rho (2j_\rho + 1)}} \frac{1}{K K'_{j_\rho}}, \tag{18b}$$

$$\theta_{j_\rho} = \frac{v_{j_\rho}}{\sqrt{N_\rho}} \frac{1}{K''_{j_\rho}}, \tag{18c}$$

$$\theta_{j_\rho j'_\rho} = u_{j_\rho} \beta_{j'_\rho j_\rho} \sqrt{\frac{10}{2j_\rho + 1}} \frac{1}{K K''_{j_\rho}}. \tag{18d}$$

The factors K, K'_{j_ρ}, and K''_{j_ρ} are defined as

$$K = \left(\sum_{j_\rho j'_\rho} \beta^2_{j_\rho j'_\rho} \right)^{1/2}, \tag{19a}$$

$$K'_{j_\rho} = \left[1 + 2 \left(\frac{v_{j_\rho}}{u_{j_\rho}} \right)^2 \frac{\langle (\hat{n}_{s_\rho} + 1) \hat{n}_{d_\rho} \rangle_{0^+_1}}{N_\rho (2j_\rho + 1)} \frac{\sum_{j'_\rho} \beta^2_{j'_\rho j_\rho}}{K^2} \right]^{1/2}, \tag{19b}$$

$$K''_{j_\rho} = \left[\frac{\langle \hat{n}_{s_\rho} \rangle_{0^+_1}}{N_\rho} + 2 \left(\frac{u_{j_\rho}}{v_{j_\rho}} \right)^2 \frac{\langle \hat{n}_{d_\rho} \rangle_{0^+_1}}{2j_\rho + 1} \frac{\sum_{j'_\rho} \beta^2_{j'_\rho j_\rho}}{K^2} \right]^{1/2}, \tag{19c}$$

where $\hat{n}_{s_\rho}$ is the number operator for the s_ρ boson and $\langle \cdots \rangle_{0^+_1}$ represents the expectation value of a given operator in the 0^+_1 ground state of the even-even nucleus. In the expressions in Eqs. (18a) to (18d), the occupation v_{j_ρ} and unoccupation u_{j_ρ} amplitudes are the same as those used in the IBFM-2 (or IBFFM-2) calculations for the odd-mass (or odd-odd) nuclei. Within this framework, no additional phenomenological parameter is introduced for the GT and Fermi operators.

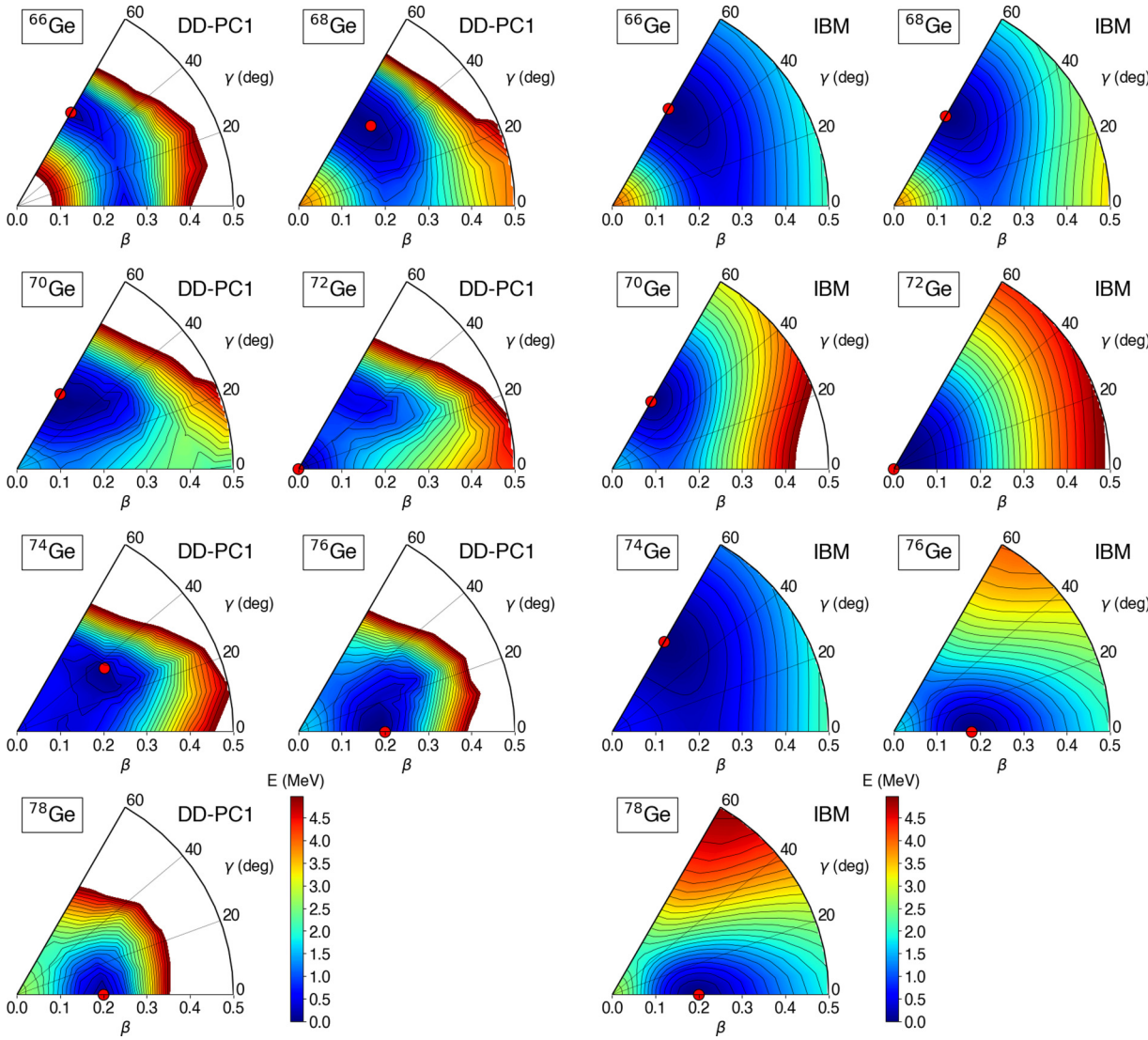

FIG. 2. SCMF and IBM (β, γ)-deformation energy surfaces for the even-even $^{66-78}$Ge nuclei. The energy difference between neighboring contours is 200 keV. The global minimum is identified by the solid circle.

For a more detailed account on the formalism of the β-decay operators within the IBFM-2, the reader is referred to Refs. [7,43,63].

III. EVEN-EVEN NUCLEI

A. Potential energy surfaces

In Fig. 2, the contour plots of the SCMF quadrupole triaxial energy surfaces for the even-even $^{66-78}$Ge nuclei are shown as functions of the (β, γ) deformations. The SCMF result indicates that the potential is generally soft in γ deformation. The softness implies a substantial degree of shape mixing near the ground state. The SCMF energy surfaces shown in the figure suggests a transition from the γ-soft oblate (^{66,68,70}Ge), to spherical-oblate shape coexistence (^{72}Ge), to γ-soft (^{74,76}Ge), and to prolate shapes (^{78}Ge). The appearance of the spherical ground-state minimum at ^{72}Ge reflects the neutron $N = 40$ subshell gap. A similar trend is obtained when another relativistic functional DD-ME2 [64] is used. The behavior of the energy surface as a function of the neutron number is also consistent with the one for the same even-even Ge nuclei, obtained in Ref. [30] with the Hartree-Fock-Bogoliubov calculations based on the Gogny-D1M [65] EDF.

The mapped IBM energy surfaces, shown also in Fig. 2, basically have a similar topology in the vicinity of the global minimum and systematic trend with N to those for the SCMF ones. A notable difference is that the IBM energy surface is rather flat in the region corresponding to large β deformations, while the SCMF one becomes even more steeper. The difference arises mainly because the IBM-2 is built on the limited configuration space consisting of valence nucleon pairs, while the SCMF model is on all the constituent nucleons [41,58]. It is also worth noting that the IBM-2 energy surface for ^{72}Ge does not reproduce the local oblate minimum that is found in the SCMF counterpart. Within the IBM, such coexisting minima can be produced, e.g., by the inclusion of the configuration mixing between the normal and intruder states [66]. This point will be discussed in Sec. III C.

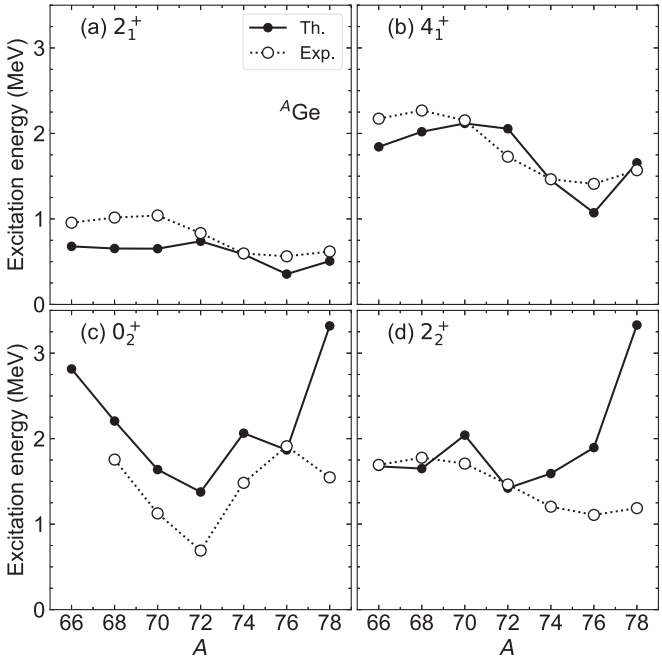

FIG. 3. Comparison of theoretical and experimental [67] excitation energies of the (a) 2_1^+, (b) 4_1^+, (c) 0_2^+, and (d) 2_2^+ states of the even-even $^{66-78}$Ge nuclei.

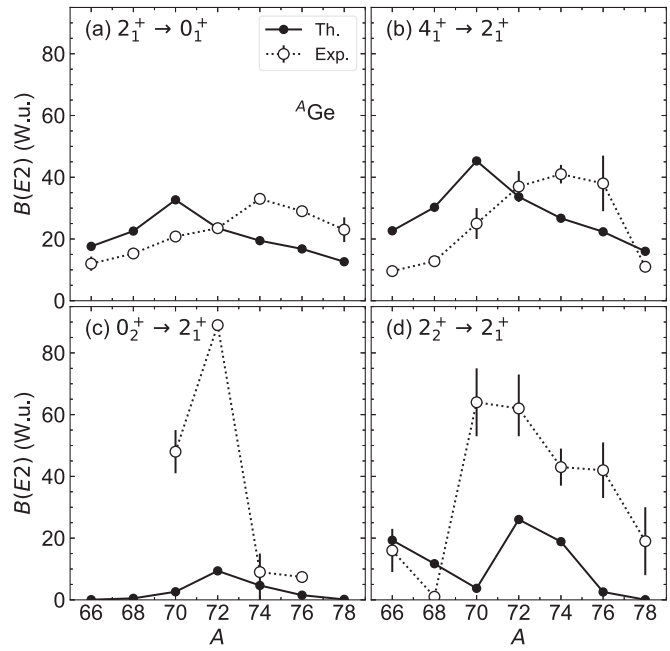

FIG. 4. Calculated and observed [67] $B(E2)$ values for the transitions (a) $2_1^+ \to 0_1^+$, (b) $4_1^+ \to 2_1^+$, (c) $0_2^+ \to 2_1^+$, and (d) $2_2^+ \to 2_1^+$.

B. Spectroscopic properties

Figure 3 shows evolution of the 2_1^+, 4_1^+, 0_2^+, and 2_2^+ energy levels for the considered even-even Ge, obtained from the diagonalization of the mapped IBM-2 Hamiltonian. In general, the calculation reproduces fairly well the observed systematics of the low-lying levels.

For ^{66,68,70}Ge, the calculation gives considerably lower 2_1^+ energy level than the experimental one [see Fig. 3(a)]. This reflects the fact that the underlying SCMF energy surface for these nuclei shows a too pronounced deformation, and then the subsequent IBM-2 calculation produces a rather rotational-like energy spectrum characterized by the too compressed 2_1^+ level. In addition, it should be kept in mind that in the present theoretical scheme the neutron-proton pair degrees of freedom are not taken into account both at the SCMF and IBM levels, which are supposed to play a certain role in those nuclei with $N \approx Z$ such as the ones considered here.

In Fig. 3(c), the calculated 0_2^+ excitation energies show a similar overall behavior to the experimental counterparts. The calculation, however, systematically overestimates the data. Especially for ^{72}Ge, the observed 0_2^+ excitation energy is rather low ($\approx$0.7 MeV), while the mapped IBM-2 overestimates it by a factor of 2. The emergence of the low-lying 0_2^+ state is often attributed to the intruder excitation, which is not taken into account in the IBM-2 framework described above.

The 2_2^+ state is, in most of the cases, considered the bandhead of the γ-vibrational band. The mapped IBM-2 reproduces the experimental data up to ^{72}Ge, but considerably overestimates the data for ^{76,78}Ge. This is also due to the fact that the SCMF energy surface shows a pronounced deformation with a steep valley in both β and γ deformations. To reproduce this topology, the derived values for the parameters χ_ν and χ_π for ^{76,78}Ge have to have large negative values, as compared to the ones for $^{68-74}$Ge (see Table I). The resulting IBM-2 spectra for ^{76,78}Ge are rather rotational like, where both the β- and γ-vibrational bands are generally high in energy with respect to the ground-state band. The other reason is that, as one approaches the neutron major shell closure $N = 50$, the model space of the IBM, which is built on the finite number of valence nucleon pairs, becomes even smaller. For instance, there are only $N_\nu = N_\pi = 2$ bosons for the nucleus ^{78}Ge, which might not be large enough to describe satisfactorily the energy levels of the nonyrast states.

Figure 4 shows the calculated $B(E2)$ values for the transitions (a) $2_1^+ \to 0_1^+$, (b) $4_1^+ \to 2_1^+$, (c) $0_2^+ \to 2_1^+$, and (d) $2_2^+ \to 2_1^+$ for the even-even Ge nuclei, compared with the experimental data [67]. The mapped IBM-2 gives maximal interband transition strengths in the ground-state band, $B(E2; 2_1^+ \to 0_1^+)$ and $B(E2; 4_1^+ \to 2_1^+)$, at ^{70}Ge. This nucleus corresponds to the middle of the major shell $N = 38$, at which the neutron boson number is maximal $N_\pi = 5$, and thus the largest quadrupole collectivity is expected. The observed values for the above $B(E2)$ transition rates, however, show a peak around ^{74}Ge. The calculated $B(E2; 0_2^+ \to 2_1^+)$ and $B(E2; 2_2^+ \to 2_1^+)$ values show a tendency similar to the observed one. The present IBM-2 calculation does not reproduce the large experimental $B(E2; 0_2^+ \to 2_1^+)$ rates for ^{70,72}Ge, mainly because it predicts for these nuclei a rather rotational-like spectrum, in which case the $0_2^+ \to 2_1^+$ transition is weak, and also because the model space does not include the effect of the configuration mixing between normal and intruder excitations.

C. Shape coexistence

Shape coexistence is expected to occur in some of the considered even-even Ge nuclei. As an illustrative example, here

the nucleus ^{72}Ge is considered, for which the spherical global minimum and an oblate local minimum are suggested to occur in the corresponding SCMF quadrupole triaxial deformation energy map.

A method to incorporate the effect of intruder configuration in the IBM-2 framework was proposed by Duval and Barrett [68]. In that method, two independent IBM-2 Hamiltonians that correspond to the normal and intruder configurations are considered. In the case of proton two-particle–two-hole excitations, for instance, the intruder configuration is regarded as a system consisting of N_ν neutron and $N_\pi + 2$ proton bosons, under the assumption that the particle-like and hole-like bosons are not distinguished from each other. The two Hamiltonians are then admixed by a specific mixing interaction. The details about the configuration mixing IBM framework are found in Ref. [68], and its application to the Ge and Se region was made in Ref. [69]. The method of Duval and Barrett was also implemented in the mapped IBM framework, and the related applications to various mass regions, including the Ge and Se ones [30], were reported [70–73].

Here, it is assumed the proton $2p-2h$ excitations occur across the $Z = 28$ major shell. The IBM-2 Hamiltonian configuration mixing (CM) is given by

$$\hat{H}_{\rm B}^{\rm CM} = \hat{\mathcal{P}}_{N_\pi}\hat{H}_{\rm B}^{N_\pi}\hat{\mathcal{P}}_{N_\pi} + \hat{\mathcal{P}}_{N_\pi+2}\big(\hat{H}_{\rm B}^{N_\pi+2} + \Delta\big)\hat{\mathcal{P}}_{N_\pi+2} + \hat{V}_{\rm mix}, \qquad (20)$$

where $\hat{H}_{\rm B}^{N_\pi+n}$ and $\hat{\mathcal{P}}_{N_\pi+n}$ $(n = 0, 2)$ are the Hamiltonian of and the projection operator onto the normal or intruder configuration space, respectively. Δ represents the energy needed to promote a proton boson across the $Z = 28$ shell closure. The form of each unperturbed Hamiltonian $\hat{H}_{\rm B}^{N_\pi+n}$ is the same as the one in Eq. (2), but a specific three-body boson term

$$\kappa'' \sum_{\rho'\neq\rho}\sum_{L}[d_\rho^\dagger \times d_\rho^\dagger \times d_{\rho'}^\dagger]^{(L)}[\tilde{d}_{\rho'} \times \tilde{d}_\rho \times \tilde{d}_\rho]^{(L)} \qquad (21)$$

is added to the Hamiltonian for the intruder configuration. The mixing interaction $\hat{V}_{\rm mix}$ in Eq. (20) is given as

$$\hat{V}_{\rm mix} = \omega(s_\pi^\dagger s_\pi^\dagger + d_\pi^\dagger d_\pi^\dagger) + ({\rm H.c.}) \qquad (22)$$

with ω mixing strength.

The coherent state for the configuration-mixing IBM is given as the direct sum of the coherent state for each unperturbed configuration. The energy surface is, in general, expressed as the 2×2 coherent-state matrix [66]. Here the lower eigenvalue of the matrix is taken as the IBM energy surface. The parameters for each unperturbed Hamiltonian is determined by associating it to each mean-field minimum: the $0p$-$0h$ Hamiltonian for the spherical global minimum, and the $2p$-$2h$ one for the oblate local minimum for ^{72}Ge. The off-set energy Δ and the mixing strength ω are determined so that the energy difference between the two mean-field minima and the barrier height for these minima are reproduced. The derived parameters are as follows: $\epsilon_d = 1.6$ MeV, $\kappa = -0.22$ MeV, $\chi_\nu = 0.30$, $\chi_\pi = 0.30$, $\kappa' = \kappa'' = 0$ MeV for the $0p$-$0h$ configuration, $\epsilon_d = 0.9$ MeV, $\kappa = -0.21$ MeV, $\chi_\nu = 0.30$, $\chi_\pi = 0.22$, $\kappa' = 0$ MeV, $\kappa'' = 0.11$ MeV for the $2p$-$2h$ configuration, $\Delta = 1.82$ MeV, and $\omega = 0.13$ MeV.

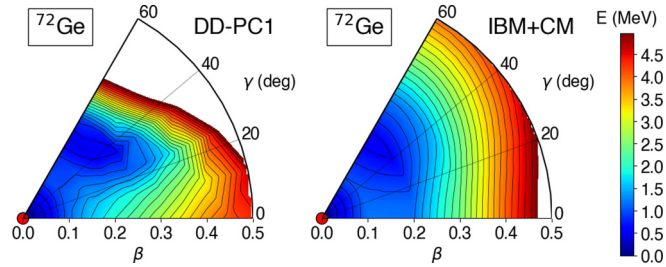

FIG. 5. Comparison of energy surfaces for ^{72}Ge calculated with the SCMF method based on the DD-PC1 functional and mapped IBM-2 that includes configuration mixing (CM).

Figure 5 compares the energy surface for the mapped IBM-2 that includes configuration mixing with the one obtained by the SCMF method. The IBM-2 surface now includes the oblate local minimum, consistent with the SCMF one. The resultant energy spectra in the cases where the configuration mixing is and is not performed are compared in Fig. 6. With the configuration mixing, the 0_2^+ energy level is significantly lowered, being close to the observed 0_2^+ level. In the configuration-mixing IBM-2 framework, the $E2$ transition operator is also extended as

$$\hat{T}^{(E2)} = \sum_{n=0,2}\sum_{\rho}\hat{\mathcal{P}}_{N_\pi+n}e^{\rho}_{{\rm B},N_\pi+n}\hat{Q}^{N_\pi+n}\hat{\mathcal{P}}_{N_\pi+n}. \qquad (23)$$

If one uses the effective charges 0.05 eb and 0.06 eb for the normal and intruder configurations, respectively, the $B(E2; 0_2^+ \to 2_1^+)$ value for ^{72}Ge is calculated to be 50 W.u. This is much greater than the value of 9.4 W.u., which is obtained without the configuration mixing, and is closer to the experimental data 89.0 ± 1.5 W.u. [67].

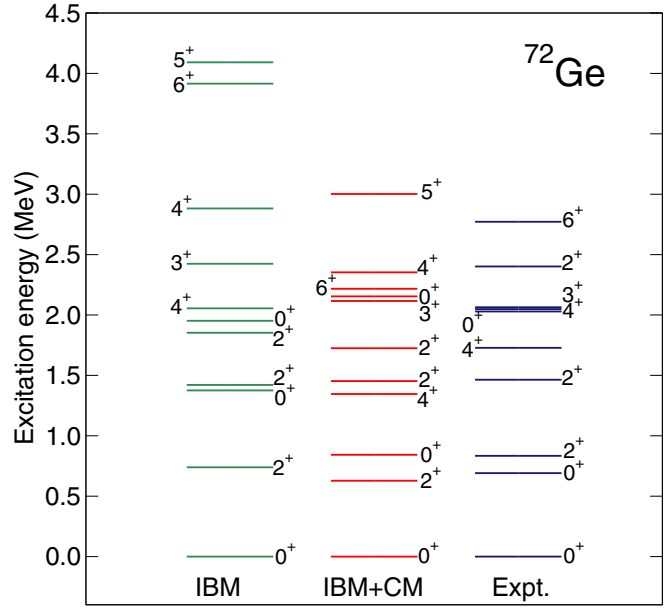

FIG. 6. Comparison of energy spectra of ^{72}Ge resulting from the mapped IBM-2 with and without the configuration mixing (CM) with the experimental spectra.

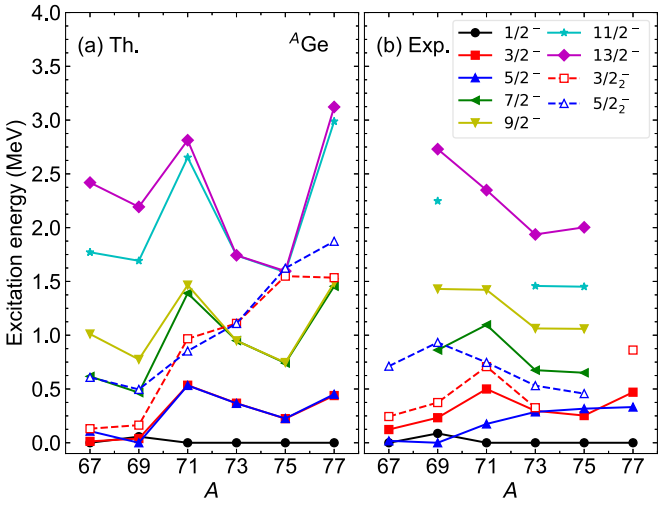

FIG. 7. Comparison of the calculated and experimental [67] low-lying negative-parity excitation spectra of the odd-N Ge nuclei.

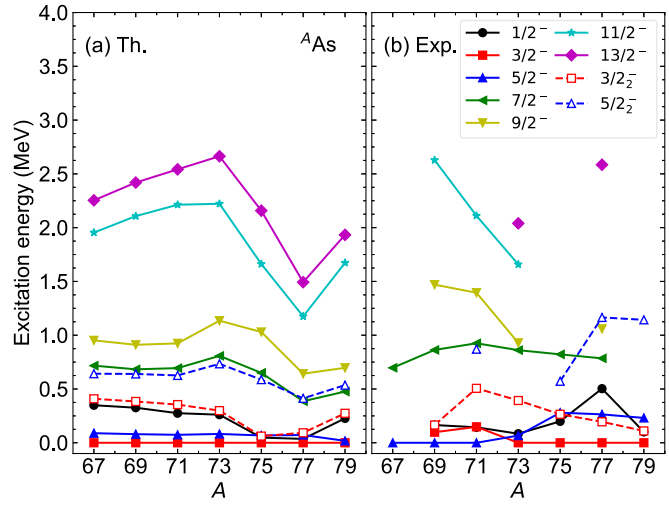

FIG. 8. Same as Fig. 7, but for the odd-Z As nuclei.

The following discussion will be, however, based on the formalism without the configuration mixing and the higher-order boson terms, since the current versions of the IBFM and IBFFM codes do not handle these effects. It remains, therefore, an open question whether the configuration mixing, as well as the higher-order boson terms, plays a role in describing the low-lying states of the neighboring odd-mass and odd-odd nuclei, and the β-decay properties.

IV. ODD-A GE AND AS NUCLEI

Figure 7 shows evolution of the low-energy negative-parity spectra of the odd-N Ge isotopes as functions of the mass number A. Both the observed and predicted low-lying level structure near the ground state rapidly changes from ^{67}Ge to ^{71}Ge, represented by the change in the ground-state spin. There appears to be a significant structural change from ^{69}Ge to ^{73}Ge. This reflects the shape transition in the neighboring even-even core Ge nuclei, particularly the neutron $N = 40$ subshell effect around ^{72}Ge. As shown in Figs. 1(c) and 1(e), the quasiparticle energies and occupation probabilities of the odd neutron also exhibit a sudden change from ^{71}Ge to ^{73}Ge.

Figure 8 gives the low-lying levels for the odd-Z As nuclei. The predicted energy levels are more stable against the mass number A, especially in the region $A \leqslant 73$, than in the case of the odd-N Ge isotopes. One also notices that the ground-state spin is predicted to be $I = 3/2$ for all the As nuclei, which disagrees with the observed one $I = 5/2^-$ for ^{67,69,71}As. These features appear because the calculated $\tilde{\epsilon}_{j_\pi}$ and $v^2_{j_\pi}$ values for the proton orbitals only gradually change with A [see Figs. 1(d) and 1(f)], and also because of the use of the constant boson-fermion strengths. Similarly to the odd-N Ge nuclei, a notable structural change in the low-lying levels is predicted to occur around ^{75,77}As, which corroborates the rapid shape evolution in the even-even Ge core nuclei (see Fig. 2). The situation is slightly different for the observed spectra, which suggest the change in the ground-state spin from ^{71}As to ^{73}As.

In Fig. 9, some predicted $B(E2)$ and $B(M1)$ transition strengths between the low-lying states for the odd-N Ge are shown. Both the calculated $B(E2)$ and $B(M1)$ values show an abrupt change within the range $69 \lesssim A \lesssim 73$, indicating that the structure of the relevant IBFM-2 wave functions change. Note that the neighboring even-even Ge nuclei also undergoes rapid structural evolution between prolate and oblate shapes.

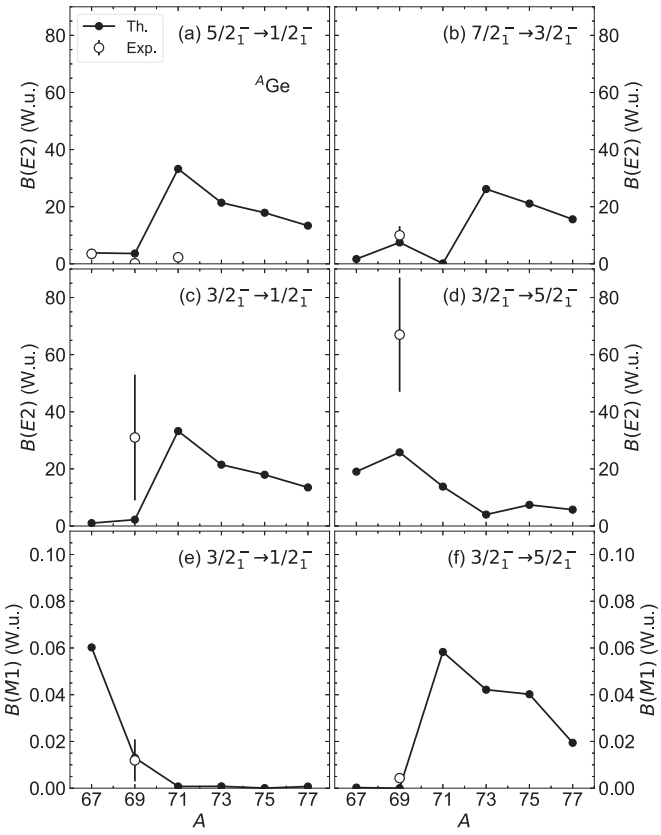

FIG. 9. Calculated $B(E2)$ and $B(M1)$ transition rates (in W.u.) between low-lying negative-parity states of odd-N Ge isotopes. The available experimental data, taken from Ref. [67], are also shown.

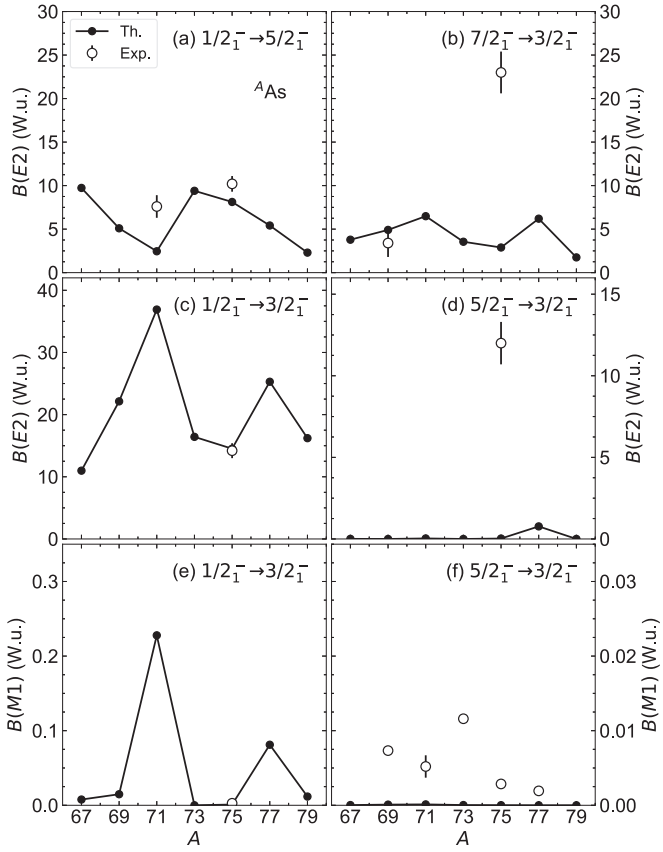

FIG. 10. Same as Fig. 9, but for the odd-Z As nuclei.

In most cases, the calculated results shown in Fig. 9 are in a reasonable agreement with the experimental data.

Figure 10 shows the $B(E2)$ and $B(M1)$ transitions between low-lying negative-parity states of the odd-Z As nuclei. One observes an irregular systematic in the predicted $B(E2;1/2_1^- \to 5/2_1^-)$, $B(E2;1/2_1^- \to 3/2_1^-)$, and $B(M1;1/2_1^- \to 3/2_1^-)$ values. The last two quantities are particularly large at ^{71}As. The occurrence of the irregularity indicates that the structure of the $1/2_1^-$ wave function obtained for ^{71}As happens to be different from the ones for the neighboring nuclei. Furthermore, both the predicted $E2$ and $M1$ rates for the $5/2_1^- \to 3/2_1^-$ transition are negligibly small, implying that the $3/2_1^-$ and $5/2_1^-$ have completely different structures in the IBFM-2.

Table III compares the calculated and experimental spectroscopic electric quadrupole $Q(I)$ and magnetic dipole $\mu(I)$ moments. In most cases, the present IBFM-2 results are in a reasonable agreement with the observed $Q(I)$ and $\mu(I)$ moments, including the sign.

To help interpreting the nature of the low-lying states in the considered odd-A systems, Fig. 11 shows the fractions of the $2p_{1/2}$, $2p_{3/2}$, and $1f_{5/2}$ single-particle configurations in the IBFM-2 wave functions for the $1/2_1^-$, $3/2_1^-$, and $5/2_1^-$ states of the odd-N Ge and odd-Z As nuclei. For ^{67,69}Ge, two or three single-particle configurations make sizable (>10%) contributions to the $1/2_1^-$ and $3/2_1^-$ wave functions. For the Ge nuclei with $A \geqslant 71$, the three states $1/2_1^-$, $3/2_1^-$, and $5/2_1^-$

TABLE III. Comparison of calculated and available experimental data for the electric quadrupole $Q(I)$ (in eb) and magnetic dipole $\mu(I)$ (in μ_N) moments of the negative-parity states with spin I for the odd-mass Ge and As nuclei. The data are taken from Ref. [74].

Nucleus	Moments	Th.	Exp.
^{67}Ge	$\mu(5/2_1^-)$	0.84	
^{69}Ge	$\mu(5/2_1^-)$	0.79	0.735 ± 0.007
^{71}Ge	$\mu(1/2_1^-)$	0.45	+0.547 ± 0.005
	$\mu(5/2_1^-)$	0.52	+1.018 ± 0.010
^{73}Ge	$\mu(5/2_1^-)$	0.76	
^{75}Ge	$\mu(1/2_1^-)$	0.45	+0.510 ± 0.005
^{77}Ge	$\mu(5/2_1^-)$	1.22	
^{69}As	$\mu(5/2_1^-)$	1.35	+1.58 ± 0.16
^{71}As	$\mu(5/2_1^-)$	1.31	(+)1.674 ± 0.02
	$Q(5/2_1^-)$	0.004	−0.017 ± 0.010
^{73}As	$\mu(5/2_1^-)$	1.38	+1.63 ± 0.10
	$Q(5/2_1^-)$	−0.02	0.356 ± 0.012
^{75}As	$\mu(3/2_1^-)$	2.85	+1.43948 ± 0.00007
	$Q(3/2_1^-)$	−0.03	+0.30 ± 0.05
	$\mu(3/2_2^-)$	0.91	+1.0 ± 0.2
	$\mu(5/2_1^-)$	1.38	+0.92 ± 0.02
	$Q(5/2_1^-)$	0.03	0.30 ± 0.10
^{77}As	$\mu(3/2_1^-)$	2.40	+1.2946 ± 0.0013
	$\mu(5/2_1^-)$	1.35	+0.74 ± 0.02
	$Q(5/2_1^-)$	0.06	<0.75

are almost entirely made of the neutron $2p_{1/2}$ configurations. This is evident from Fig. 1(c), in which there is a larger energy gap between the $2p_{1/2}$ and the $2p_{3/2}$ and $1f_{5/2}$ quasineutron energies for the odd-A Ge with $A \geqslant 73$ than for the ones with $A \leqslant 71$. The $3/2_1^-$ and $5/2_1^-$ states of the odd-Z As nuclei are mostly accounted for by the proton $2p_{3/2}$ and $1f_{5/2}$ configurations, respectively. This explains the vanishing $B(E2;5/2_1^- \to 3/2_1^-)$ and $B(M1;5/2_1^- \to 3/2_1^-)$ rates, shown in Figs. 10(d) and 10(f). As seen in Fig. 11(b), for the odd-Z As nuclei the largest contribution (≈60%) to the $1/2_1^-$ wave function is from the $2p_{3/2}$ configuration, while either the $2p_{1/2}$ or $1f_{5/2}$ configuration constitutes about 30% of the wave function. Also, the $1/2_1^-$ wave function for ^{71}As has a different composition from the ones for the neighboring isotopes, and this explains the irregular behavior of those calculated $B(E2)$ and $B(M1)$ values that involve the $1/2_1^-$ state [see Figs. 10(a), 10(c), and 10(e)].

V. ODD-ODD AS NUCLEI

Figure 12 shows the results for the low-energy positive-parity spectra for the odd-odd As nuclei, obtained with the IBFFM-2. For those nuclei with mass $A \geqslant 72$, the observed ground-state spin of $I = 1^+$ is reproduced. The corresponding IBFFM-2 1_1^+ wave functions for these nuclei are dominated (approximately 80%) by the neutron-proton pair component $[\nu p_{1/2} \otimes \pi p_{3/2}]^{J=1^+}$ coupled to the even-even boson core nuclei. This configuration plays a less important role in the predicted 1_1^+ ground states for ^{68,70}As. Instead, several configurations are admixed in these nuclei, with the major contributions coming from the components $[\nu f_{5/2} \otimes$

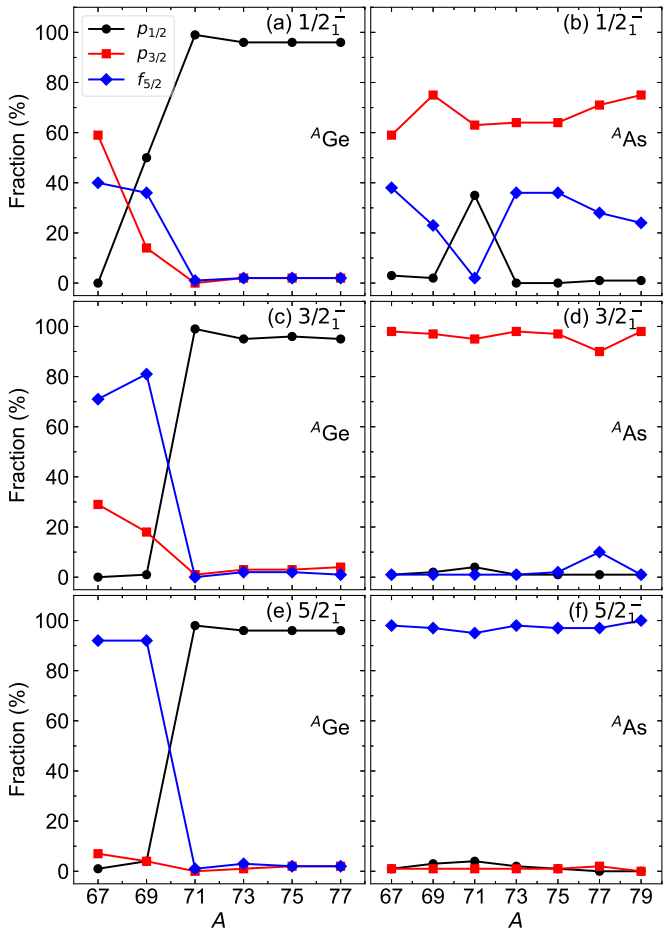

FIG. 11. Fractions of the $2p_{1/2}$, $2p_{3/2}$, and $1f_{5/2}$ single-particle configurations in the IBFM-2 wave functions for the $1/2_1^-$, $3/2_1^-$, and $5/2_1^-$ states of the odd-N Ge and odd-Z As nuclei.

$\pi p_{3/2}]^{J=3^+}$ (40%), $[\nu p_{3/2} \otimes \pi p_{3/2}]^{J=2^+}$ (16%), and $[\nu f_{5/2} \otimes \pi p_{3/2}]^{J=1^+}$ (13%) for ^{68}As, and $[\nu f_{5/2} \otimes \pi p_{3/2}]^{J=1^+}$ (44%), $[\nu p_{1/2} \otimes \pi p_{3/2}]^{J=1^+}$ (12%), and $[\nu f_{5/2} \otimes \pi p_{3/2}]^{J=3^+}$ (10%) for ^{70}As.

Here, the IBFFM-2 does not reproduce for ^{68}As and ^{70}As the observed ground state spins of $I = 3^+$ and 4^+, respectively. For ^{68}As, main contributions to the IBFFM-2 wave function of the 3_1^+ state come from the pair components $[\nu f_{5/2} \otimes \pi p_{3/2}]^{J=3^+}$ (70%), and $[\nu f_{5/2} \otimes \pi f_{5/2}]^{J=3^+}$ (11%). For both ^{68}As and ^{70}As, $[\nu f_{5/2} \otimes \pi f_{5/2}]^{J=4^+}$ constitutes approximately 75% of the 4_1^+ wave function. For the $A \geqslant 72$ Ge nuclei, the configuration $[\nu p_{1/2} \otimes \pi f_{5/2}]^{J=3^+}$ accounts for $\approx$70% of the wave functions for both the 3_1^+ and 4_1^+ states.

Table IV lists the calculated $Q(I)$ and $\mu(I)$ moments for the odd-odd As nuclei, as compared with the available experimental data [74]. The observed moments, especially their sign, are reasonably reproduced by the IBFFM-2.

VI. β DECAY

The ft values for the β decays of the odd-A As into Ge nuclei, and of the even-A As into Ge nuclei, and vice versa,

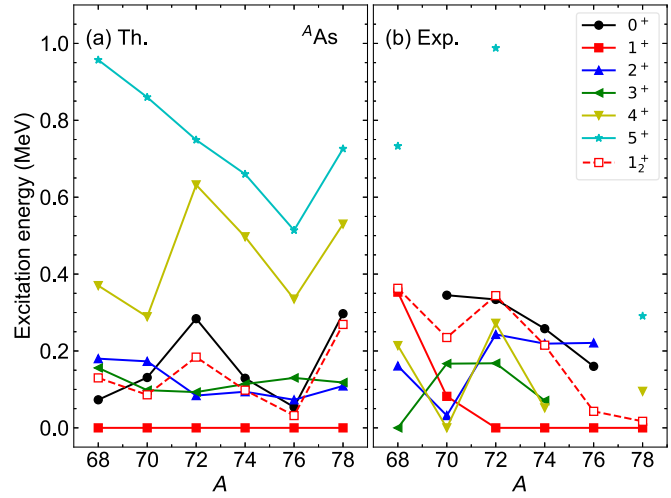

FIG. 12. Same as Fig. 7, but for the low-energy positive-parity states of odd-odd As nuclei.

are computed by the formula

$$ft = \frac{K}{|M(\mathrm{F})|^2 + \left(\frac{g_\mathrm{A}}{g_\mathrm{V}}\right)^2 |M(\mathrm{GT})|^2}, \tag{24}$$

where the constant $K = 6163$ sec, and $M(\mathrm{F})$ and $M(\mathrm{GT})$ are the reduced matrix elements of the Fermi $\hat{T}^{\mathrm{F}}$ (14) and Gamow-Teller $\hat{T}^{\mathrm{GT}}$ (13) operators, respectively. The free values of the vector and axial vector coupling constants $g_\mathrm{V} = 1$ and $g_\mathrm{A} = 1.27$, respectively, are used.

A. β decays between odd-A nuclei

Figure 13 shows the calculated $\log ft$ values for the electron-capture (EC) decays of the $5/2_1^-$ and $3/2^-$ states of the odd-A As nuclei, and for the β^- decays of the $1/2_1^-$ state of the odd-A Ge nuclei. The behaviours of the predicted $\log ft$ values reflect evolution of the underlying nuclear structure. A characteristic kink is observed at $A = 71$ in the calculated $\log ft$ values for the $\Delta I = 0$ decays As $(5/2_1^-) \rightarrow$ Ge $(5/2_1^-)$ and Ge $(1/2_1^-) \rightarrow$ As $(1/2_1^-)$, shown in Figs. 13(a) and 13(d), respectively. The

TABLE IV. Same as Table III, but for the positive-parity states of odd-odd As nuclei.

Nucleus	Moments	Th.	Exp.
^{68}As	$Q(3_1^+)$	0.02	
	$\mu(3_1^+)$	2.13	
^{70}As	$Q(4_1^+)$	0.10	$+0.09 \pm 0.02$
	$\mu(4_1^+)$	1.72	$+2.1061 \pm 0.0002$
^{72}As	$Q(3_1^+)$	0.07	
	$\mu(1_1^+)$	1.92	
	$\mu(3_1^+)$	1.38	$+1.58 \pm 0.02$
^{74}As	$\mu(1_1^+)$	2.10	
	$\mu(4_1^+)$	1.94	$+3.24 \pm 0.04$
^{76}As	$\mu(1_1^+)$	1.71	$+0.559 \pm 0.005$
^{78}As	$\mu(1_1^+)$	2.44	

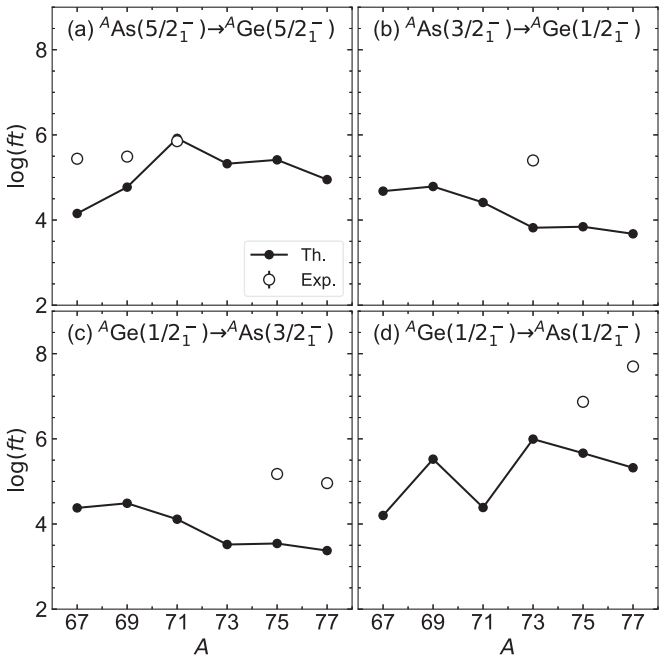

FIG. 13. Calculated log ft values for the electron-capture decays from the odd-A As to Ge nuclei, (a) $5/2_1^- \rightarrow 5/2_1^-$ and (b) $3/2_1^- \rightarrow 1/2_1^-$, and the β^- decays from the odd-A Ge to As nuclei, (c) $1/2_1^- \rightarrow 3/2_1^-$ and (d) $1/2_1^- \rightarrow 1/2_1^-$. The experimental data, available from Ref. [67], are also shown.

log ft results for the GT-type ($\Delta I = 1$) decays As $(3/2_1^-) \rightarrow$ Ge $(1/2_1^-)$ and Ge $(1/2_1^-) \rightarrow$ As $(3/2_1^-)$ rather abruptly decrease from $A = 71$ to 73.

As shown in Fig. 13 the calculation systematically underestimates the observed log ft values [67]. For both the ^{67,69}As $(5/2_1^-) \rightarrow {}^{67,69}$Ge $(5/2_1^-)$ decays, the dominant contributions to the GT and Fermi matrix elements come from the terms of the type $(a^\dagger_{\nu f_{5/2}} \times a_{\pi f_{5/2}})^{(I)}$, with $I = 1$ and 0, respectively. As one can see in Figs. 11(e) and 11(f), the $5/2_1^-$ states of both the parent (^{67,69}As) and daughter (^{67,69}Ge) nuclei are almost purely made of the $1f_{5/2}$ single-particle configurations, hence the GT and Fermi transitions are calculated to be so large as to give the small log ft values compared to the data.

For the GT-type decay ^{73}As $(3/2_1^-) \rightarrow {}^{73}$Ge $(1/2_1^-)$, the largest contribution to the GT strength is from the term proportional to $s_\nu(a^\dagger_{\nu p_{1/2}} \times a_{\pi p_{3/2}})^{(1)}$. The IBFM-2 wave functions for the $3/2_1^-$ parent state of ^{73}As and the $1/2_1^-$ daughter state of ^{73}Ge are built predominantly on the $2p_{3/2}$ and $2p_{1/2}$ single-proton configurations, respectively [see Figs. 11(a) and 11(d)]. Thus the GT strength between these states is calculated to be substantially large, hence the small log ft value is obtained.

The rapid increase of the log ft values for As $(5/2_1^-) \rightarrow$ Ge $(5/2_1^-)$ decay toward $A = 71$ is attributed to the fact that the structure of the wave function for the $5/2_1^-$ daughter state drastically changes from $A = 69$ to 71. One finds from Figs. 11(e) and 11(f) that, the parent ^{71}As $(5/2_1^-)$ and the daughter ^{71}Ge $(5/2_1^-)$ states are here almost purely made of the proton $1f_{5/2}$ and neutron $2p_{1/2}$ single-particle configurations, respectively. Thus the terms such as $(a^\dagger_{\nu f_{5/2}} \times a_{\pi f_{5/2}})^{(I=0,1)}$, which make a large contribution to the GT and Fermi matrix elements for the decays of ^{67,69}As, now play a much less important role in the case of the ^{71}As decay. There are, instead, various other terms with small amplitudes in the GT and Fermi matrix elements of the ^{71}As decay, which cancel each other and lead to the large log ft value as compared to the ^{67,69}As decays.

TABLE V. Comparison of calculated and observed [67] log ft values for the EC decays from odd-A As to Ge nuclei.

		log ft	
Decay	$I \rightarrow I'$	Th.	Exp.
^{67}As $\rightarrow$ ^{67}Ge	$5/2_1^- \rightarrow 5/2_1^-$	4.15	5.44 ± 0.13
	$5/2_1^- \rightarrow 5/2_2^-$	6.63	5.92 ± 0.08[a]
	$5/2_1^- \rightarrow 5/2_3^-$	6.08	6.4 ± 0.4[a]
	$5/2_1^- \rightarrow 3/2_1^-$	6.49	6.18 ± 0.11[a]
	$5/2_1^- \rightarrow 3/2_2^-$	7.61	5.64 ± 0.07[a]
^{69}As $\rightarrow$ ^{69}Ge	$5/2_1^- \rightarrow 5/2_1^-$	4.77	5.49 ± 0.02
	$5/2_1^- \rightarrow 5/2_2^-$	6.92	6.94 ± 0.07
	$5/2_1^- \rightarrow 5/2_3^-$	5.63	6.80 ± 0.06
	$5/2_1^- \rightarrow 5/2_4^-$	5.98	6.47 ± 0.06
	$5/2_1^- \rightarrow 5/2_5^-$	7.15	5.95 ± 0.05
	$5/2_1^- \rightarrow 3/2_1^-$	7.58	6.05 ± 0.02
	$5/2_1^- \rightarrow 3/2_2^-$	7.44	7.21 ± 0.05
	$5/2_1^- \rightarrow 3/2_3^-$	6.43	6.71 ± 0.06
	$5/2_1^- \rightarrow 3/2_4^-$	7.07	5.82 ± 0.05
	$5/2_1^- \rightarrow 3/2_5^-$	8.00	6.21 ± 0.05
	$5/2_1^- \rightarrow 7/2_1^-$	10.85	6.20 ± 0.05
	$5/2_1^- \rightarrow 7/2_2^-$	7.46	5.44 ± 0.05
^{71}As $\rightarrow$ ^{71}Ge	$5/2_1^- \rightarrow 5/2_1^-$	5.92	5.853 ± 0.012
	$5/2_1^- \rightarrow 5/2_2^-$	6.28	
	$5/2_1^- \rightarrow 5/2_3^-$	6.55	6.869 ± 0.015
	$5/2_1^- \rightarrow 5/2_4^-$	7.74	9.14 ± 0.08[b]
	$5/2_1^- \rightarrow 5/2_5^-$	7.30	6.840 ± 0.025
	$5/2_1^- \rightarrow 3/2_1^-$	6.74	7.192 ± 0.012
	$5/2_1^- \rightarrow 3/2_2^-$	7.47	>8.6
	$5/2_1^- \rightarrow 3/2_3^-$	7.24	6.333 ± 0.013
	$5/2_1^- \rightarrow 3/2_4^-$	8.25	7.430 ± 0.023
	$5/2_1^- \rightarrow 3/2_5^-$	8.10	6.946 ± 0.014
	$5/2_1^- \rightarrow 7/2_1^-$	8.38	8.79 ± 0.25
	$5/2_1^- \rightarrow 7/2_2^-$	7.85	7.296 ± 0.016
^{73}As $\rightarrow$ ^{73}Ge	$3/2_1^- \rightarrow 1/2_1^-$	3.82	5.4

[a]Parity not firmly established.
[b]$I = (3/2, 5/2^-)$ level at 886 keV.

As shown in Figs. 13(c) and 13(d), the calculated log ft values for the β^- decays Ge $(1/2_1^-) \rightarrow$ As $(3/2_1^-)$ and Ge $(1/2_1^-) \rightarrow$ As $(1/2_1^-)$, show a certain systematic trend with A. Such behaviours also reflect the structure of the IBFM-2 wave functions for the parent and daughter states.

For the sake of completeness, Tables V and VI show the calculated and experimental log ft values for those β decays for which the data are available.

One can also make a comparison with the previous IBFM-2 calculation for the ^{69,71}As $\rightarrow$ ^{69,71}Ge β decays in Ref. [8]. In general, the log ft values obtained in the present study appear to be systematically larger than those reported in Ref. [8]. Particularly for the decay ^{69}As $(5/2_1^-) \rightarrow {}^{69}$Ge $(3/2_1^-)$, here

TABLE VI. Same as Table V, but for the β^- decays from odd-A Ge to As nuclei.

Decay	$I \to I'$	log ft Th.	log ft Exp.
^{75}Ge $\to$ ^{75}As	$1/2_1^- \to 3/2_1^-$	3.54	5.175 ± 0.007
	$1/2_1^- \to 3/2_2^-$	5.04	5.63 ± 0.05
	$1/2_1^- \to 3/2_3^-$	5.90	6.42 ± 0.06[a]
	$1/2_1^- \to 1/2_1^-$	5.66	6.87 ± 0.05
	$1/2_1^- \to 1/2_2^-$	4.45	6.94 ± 0.05
	$1/2_1^- \to 1/2_3^-$	7.18	6.42 ± 0.06[a]
^{77}Ge $\to$ ^{77}As	$1/2_1^- \to 3/2_1^-$	3.38	4.96 ± 0.04
	$1/2_1^- \to 3/2_2^-$	3.79	7.2 ± 0.2
	$1/2_1^- \to 3/2_3^-$	4.71	5.3 ± 0.1
	$1/2_1^- \to 3/2_4^-$	4.82	7.2 ± 0.1
	$1/2_1^- \to 3/2_5^-$	5.15	5.7 ± 0.1[b]
	$1/2_1^- \to 1/2_1^-$	5.32	7.7 ± 0.1
	$1/2_1^- \to 1/2_2^-$	4.91	5.7 ± 0.1[b]
	$1/2_1^- \to 1/2_3^-$	3.98	5.8 ± 0.1[c]

[a] $I = 1/2^-$ or $3/2^-$ state at 618 keV.
[b] $I = 1/2^-$ or $3/2^-$ state at 1605 keV.
[c] $I = 1/2^-$ or $3/2^-$ state at 1676 keV.

the value log $ft = 7.58$ is obtained, which overestimates the experimental one, 6.05 ± 0.02. On the other hand, the calculation in Ref. [8] gave a smaller value log $ft = 5.88$, in a better agreement with experiment. The log ft values for the $\Delta I = 0$ decay ^{69}As $(5/2_1^-) \to$ ^{69}Ge $(5/2_1^-)$ obtained from both calculations are close to each other, i.e., log $ft = 4.26$ in Ref. [8] and the present one is slightly larger, log $ft = 4.77$. Both calculations underestimate the data, log $ft = 5.49 \pm 0.02$. For both IBFM-2 calculations, the results for the log ft values appear to be quite sensitive to the wave functions for the initial and final odd-A nuclei. In fact, the IBFM-2 framework in Ref. [8] is largely based on the phenomenological grounds, i.e., the empirical parameters for the even-even IBM-2 core Hamiltonian, and the phenomenological single-particle energies were adopted in that reference, while most of the parameters are here determined based on the EDF calculations.

To make a reasonable comparison with the experimental log ft data, one could estimate the effective value of the g_A/g_V ratio for the GT matrix element [see Eq. (24)], denoted here by $(g_A/g_V)_{\rm eff}$. By fitting to the experimental log ft value for the $\Delta I = 1$ β-decay ^{73}As $(3/2_1^-) \to$ ^{73}Ge $(1/2_1^-)$ one obtains $(g_A/g_V)_{\rm eff} = 0.206$, equivalent to a quenching factor $q = 0.162$. If one applies this $(g_A/g_V)_{\rm eff}$ value, for instance, to the $\Delta I = 0$ decay ^{69}As $(5/2_1^-) \to$ ^{69}Ge $(5/2_1^-)$, then the log ft value is only slightly increased to log $ft = 5.06$, with respect to the one (4.77) obtained with the free g_A/g_V ratio. Likewise, the $(g_A/g_V)_{\rm eff}$ values for the ^{75}Ge $(1/2_1^-) \to$ ^{75}As $(3/2_1^-)$ and ^{75}Ge $(1/2_1^-) \to$ ^{75}As $(3/2_1^-)$ decays are calculated to be 0.194 and 0.204, respectively. Also in these cases, the quenching of the g_A/g_V ratio does not drastically increase the relevant $\Delta I = 0\beta$ decay, i.e., the $1/2_1^- \to 1/2_1^-$ one.

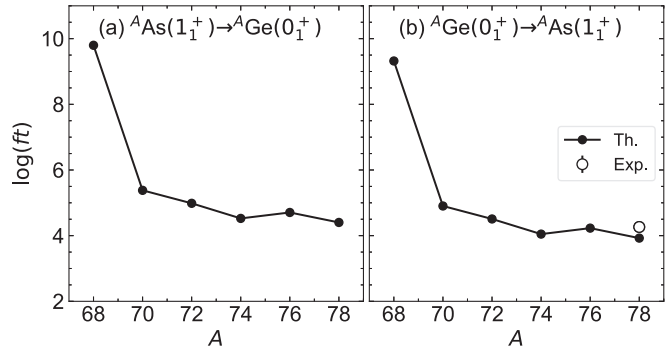

FIG. 14. Same as Fig. 13, but for the β^+/EC decay $1_1^+ \to 0_1^+$ from the even-A As to Ge nuclei (a), and the β^- decay $0_1^+ \to 1_1^+$ from the even-A Ge to As nuclei (b).

B. β decays between even-A nuclei

In Fig. 14 shown are the calculated log ft values for the GT-type transitions between the even-A nuclei, i.e., As $(1_1^+) \to$ Ge (0_1^+) β^+/EC and Ge $(0_1^+) \to$ As (1_1^+) β^- decays. The present calculation gives the values typically within the range $4 \lesssim \log ft \lesssim 5$ for both the β^+/EC and β^- decays. Apart from the decays of ^{68}As and ^{68}Ge, the predicted log ft values show a gradual decrease with A, but with a kink at $A = 76$. Note that a good agreement with the observed log ft value is seen for the β^- decay ^{78}Ge $(0_1^+) \to$ ^{78}As (1_1^+) [see Fig. 14(b)]. As shown in Sec. V, the IBFFM-2 wave functions for the 1_1^+ state of those odd-odd As nuclei with $A \geqslant 72$ are dominated by the neutron-proton pair configuration $[\nu p_{1/2} \otimes \pi p_{3/2}]^{J=1^+}$. For the GT transitions between those nuclei with $A \geqslant 72$, components in the GT operator of the forms proportional to $(a^\dagger_{\nu p_{1/2}} \times a^\dagger_{\pi p_{3/2}})^{(1)}$, $(a^\dagger_{\nu p_{3/2}} \times a^\dagger_{\pi p_{1/2}})^{(1)}$, and $(a^\dagger_{\nu p_{3/2}} \times a^\dagger_{\pi p_{3/2}})^{(1)}$ have particularly large contributions to the β-decay rates.

On the other hand, as mentioned above, the calculation predicts exceptionally large log ft values ($\approx$9–10) for the decays of the states ^{68}As (1_1^+) and ^{68}Ge (0_1^+). This is, to a large extent, traced back to the IBFFM-2 wave function of the 1_1^+ state of the ^{68}As nucleus, in which the fraction of the component $[\nu p_{1/2} \otimes \pi p_{3/2}]^{J=1^+}$ is negligibly small, in comparison to the decays of the $A \geqslant 72$ nuclei. In the GT matrix elements, the terms corresponding to the coupling between the neutron $2p_{1/2}$ (or $2p_{3/2}$) and proton $2p_{3/2}$ (or $2p_{1/2}$) single-particle states make only vanishing contributions, while other terms have small amplitudes and cancel each other.

Table VII shows a comparison between the calculated and experimental data for the β-decay log ft values for the ground states of even-A nuclei. The predicted log ft values for the relevant β decays, i.e., ^{68}As $(3_1^+) \to$ ^{68}Ge (2_1^+), ^{68}As $(3_1^+) \to$ ^{68}Ge (4_1^+), ^{70}As $(4_1^+) \to$ ^{70}Ge (4_1^+), and ^{78}Ge $(0_1^+) \to$ ^{78}Ge (1_1^+), are generally in a fair agreement with the observed ones. The IBFFM-2 log ft values for the ^{70}As $(4_1^+) \to$ ^{70}Ge (3_1^+) decay is nearly twice as large as the observed one. The large deviation is probably related to the fact that the IBFFM-2 calculation does not give the correct ground-state spin of $I = 4^+$ for ^{70}As. For this particular decay, numerous terms are fragmented and cancel each other

TABLE VII. Same as Table V, but for the β^+/EC decays from even-A As to Ge nuclei, and for the β^- decays from ^{78}Ge to ^{78}As.

		log ft	
Decay	$I \to I'$	Th.	Exp.
^{68}As $\to$ ^{68}Ge	$3_1^+ \to 2_1^+$	6.66	7.38 ± 0.24
	$3_1^+ \to 2_2^+$	6.95	6.86 ± 0.19
	$3_1^+ \to 2_3^+$	6.34	6.89 ± 0.10
	$3_1^+ \to 2_4^+$	5.81	7.24 ± 0.04
	$3_1^+ \to 2_5^+$	7.21	6.57 ± 0.04
	$3_1^+ \to 4_1^+$	6.34	7.02 ± 0.06
	$3_1^+ \to 4_2^+$	5.73	6.74 ± 0.03
	$3_1^+ \to 4_3^+$	6.63	5.979 ± 0.018[a]
^{70}As $\to$ ^{70}Ge	$4_1^+ \to 4_1^+$	6.58	7.30 ± 0.16
	$4_1^+ \to 4_2^+$	6.03	7.37 ± 0.14
	$4_1^+ \to 4_3^+$	6.01	5.69 ± 0.05
	$4_1^+ \to 3_1^+$	10.74	6.97 ± 0.04
^{78}Ge $\to$ ^{78}As	$0_1^+ \to 1_1^+$	3.92	4.264 ± 0.025
	$0_1^+ \to 1_2^+$	5.15	5.61 ± 0.12

[a]Level at 3042 keV with spin and parity temporarily assigned to be (4^+).

in the GT matrix element, giving rise to the too large log ft value.

By following the same procedure as discussed in the previous section, the $(g_A/g_V)_{\text{eff}}$ ratios can be extracted for the β decays of the even-A nuclei. Of particular interest is the ^{78}Ge $(0_1^+) \to$ ^{78}As (1_1^+) β^- decay, since the neighboring nucleus ^{76}Ge is a candidate for the $0\nu\beta\beta$-decay emitter. For the above decay, one obtains the effective ratio $(g_A/g_V)_{\text{eff}} = 0.860$, corresponding to the quenching factor $q = 0.677$. This appears to be a modest value, as compared with those obtained here for the β decays of odd-A nuclei. The result is also more or less consistent with a common value of the effective $(g_A/g_V)_{\text{eff}}$ ratio that is often considered in many of the calculations for the single-β and $\beta\beta$ decays of ^{76}Ge [20]. One also obtains the $(g_A/g_V)_{\text{eff}}$ values for the ^{68}As decays. For instance, the value $(g_A/g_V)_{\text{eff}} = 0.554$ is extracted for the $3_1^+ \to 2_1^+$ decay.

VII. CONCLUDING REMARKS

The shape evolution and the related spectroscopic properties of the low-lying states, and the β-decay properties of the even-even, odd-mass, and odd-odd Ge and As nuclei in the mass $A \approx 70$–80 region have been investigated within the framework of the nuclear EDF and the particle-boson coupling scheme. The constrained SCMF calculation based on the universal relativistic functional DD-PC1 and the separable pairing force of finite range provides triaxial quadrupole deformation energy surface for the even-even $^{66-78}$Ge nuclei. By mapping the mean-field energy surface onto the expectation value of the IBM-2 Hamiltonian in the coherent state, the parameters for the Hamiltonian have been determined. The same SCMF calculation yields spherical single(quasi)-particle energies and occupation probabilities, which are the essential building blocks of the particle-boson interactions, and the Gamow-Teller and Fermi transition operators. Fixed values are employed for the three coupling constants for the particle-boson interaction terms, and for the two parameters for the residual neutron-proton interaction in the IBFFM-2, which are determined to have an overall reasonable agreement with the low-energy data for the odd-A and odd-odd nuclei under study.

At the SCMF level, a rapid nuclear structural evolution as a function of the nucleon number has been suggested in the energy surface, from the γ-soft oblate shapes for $^{66-70}$Ge, to the spherical-oblate shape coexistence for ^{72}Ge, to the triaxial deformation for ^{74}Ge, and to the γ-soft prolate shapes for ^{76,78}Ge. The resultant energy spectra for the low-lying states, obtained by the diagonalization of the mapped IBM-2 Hamiltonian, follow the observed systematics with A. The possibility of shape coexistence for ^{72}Ge has been addressed, in which nucleus the observed spectrum is characterized by the low-lying excited 0^+ state below the 2_1^+ one. The configuration-mixing IBM-2 calculation reproduces well the observed 0_2^+ excitation energy. The calculated low-lying negative-parity levels in the neighboring odd-N Ge and odd-Z As, as well as the odd-odd As, nuclei show the systematic behaviours reflecting the shape transition that is suggested to occur in the even-even Ge core. The $B(E2)$ and $B(M1)$ transition rates in the odd-nucleon systems are, however, sensitive to the IBFM-2 or IBFFM-2 wave functions.

The wave functions for the even- and odd-A nuclei have been then used to compute the GT and Fermi matrix elements for the β decays. The predicted log ft values for the β decays of the odd-A nuclei evolve with A, corroborating the underlying nuclear structure evolution in the parent and daughter nuclear systems. As compared to experiment, the log ft values obtained for the odd-A nuclei are systematically small. This reflects the nature of the corresponding IBFM-2 wave functions and, in turn, serves as a sensitive test of various model assumptions and the microscopic input provided by the EDF. To effectively account for the deviation between the IBFM-2 and observed log ft values, drastic quenching for the ratio g_A/g_V would be required for the odd-A cases. For the decays of the even-A As and Ge nuclei, the agreement with the experimental log ft values has turned out to be slightly better, and rather modest quenching has been suggested.

The present theoretical scheme allows for a simultaneous and computationally feasible calculation of the low-lying states and their β decays for all kinds of nuclei, i.e., even-even, odd-mass, and odd-odd ones, based largely on the nuclear EDF calculations. The next step is the applications of the methodology to the β-decay properties of more neutron-rich nuclei, which are expected to play a significant role in the astrophysical processes and are experimentally of much interest. On the other hand, the reported spectroscopic calculation in this mass region opens up a possibility to study the effects of the shape coexistence, as well as the triaxial deformation, on the low-lying states of the odd-nucleon systems within the IBFM-2 and IBFFM-2, and on the predictions on their β decays. These would require a major extension of the model. Work along these lines is in progress, and will be reported elsewhere.

ACKNOWLEDGMENTS

This work is financed within the Tenure Track Pilot Programme of the Croatian Science Foundation and the École Polytechnique Fédérale de Lausanne, and Project No. TTP-2018-07-3554 Exotic Nuclear Structure and Dynamics, with funds of the Croatian-Swiss Research Programme.

[1] I. Dillmann, K.-L. Kratz, A. Wöhr, O. Arndt, B. A. Brown, P. Hoff, M. Hjorth-Jensen, U. Köster, A. N. Ostrowski, B. Pfeiffer, D. Seweryniak, J. Shergur, and W. B. Walters (ISOLDE Collaboration), Phys. Rev. Lett. **91**, 162503 (2003).

[2] S. Nishimura, Z. Li, H. Watanabe, K. Yoshinaga, T. Sumikama, T. Tachibana, K. Yamaguchi, M. Kurata-Nishimura, G. Lorusso, Y. Miyashita, A. Odahara, H. Baba, J. S. Berryman, N. Blasi, A. Bracco, F. Camera, J. Chiba, P. Doornenbal, S. Go, T. Hashimoto *et al.*, Phys. Rev. Lett. **106**, 052502 (2011).

[3] M. Quinn, A. Aprahamian, J. Pereira, R. Surman, O. Arndt, T. Baumann, A. Becerril, T. Elliot, A. Estrade, D. Galaviz, T. Ginter, M. Hausmann, S. Hennrich, R. Kessler, K.-L. Kratz, G. Lorusso, P. F. Mantica, M. Matos, F. Montes, B. Pfeiffer *et al.*, Phys. Rev. C **85**, 035807 (2012).

[4] G. Lorusso, S. Nishimura, Z. Y. Xu, A. Jungclaus, Y. Shimizu, G. S. Simpson, P.-A. Söderström, H. Watanabe, F. Browne, P. Doornenbal, G. Gey, H. S. Jung, B. Meyer, T. Sumikama, J. Taprogge, Z. Vajta, J. Wu, H. Baba, G. Benzoni, K. Y. Chae *et al.*, Phys. Rev. Lett. **114**, 192501 (2015).

[5] R. Caballero-Folch, C. Domingo-Pardo, J. Agramunt, A. Algora, F. Ameil, A. Arcones, Y. Ayyad, J. Benlliure, I. N. Borzov, M. Bowry, F. Calviño, D. Cano-Ott, G. Cortés, T. Davinson, I. Dillmann, A. Estrade, A. Evdokimov, T. Faestermann, F. Farinon, D. Galaviz *et al.*, Phys. Rev. Lett. **117**, 012501 (2016).

[6] P. Navrátil and J. Dobes, Phys. Rev. C **37**, 2126 (1988).

[7] F. Dellagiacoma and F. Iachello, Phys. Lett. B **218**, 399 (1989).

[8] S. Brant, N. Yoshida, and L. Zuffi, Phys. Rev. C **70**, 054301 (2004).

[9] N. Yoshida and F. Iachello, Prog. Theor. Exp. Phys. **2013**, 043D01 (2013).

[10] E. Mardones, J. Barea, C. E. Alonso, and J. M. Arias, Phys. Rev. C **93**, 034332 (2016).

[11] K. Nomura, R. Rodríguez-Guzmán, and L. M. Robledo, Phys. Rev. C **101**, 024311 (2020).

[12] K. Nomura, R. Rodríguez-Guzmán, and L. M. Robledo, Phys. Rev. C **101**, 044318 (2020).

[13] J. Ferretti, J. Kotila, R. I. Magaña Vsevolodovna, and E. Santopinto, Phys. Rev. C **102**, 054329 (2020).

[14] R. Álvarez-Rodríguez, P. Sarriguren, E. Moya de Guerra, L. Pacearescu, A. Faessler, and F. Šimkovic, Phys. Rev. C **70**, 064309 (2004).

[15] P. Sarriguren, Phys. Rev. C **91**, 044304 (2015).

[16] J. M. Boillos and P. Sarriguren, Phys. Rev. C **91**, 034311 (2015).

[17] P. Pirinen and J. Suhonen, Phys. Rev. C **91**, 054309 (2015).

[18] F. Šimkovic, V. Rodin, A. Faessler, and P. Vogel, Phys. Rev. C **87**, 045501 (2013).

[19] M. T. Mustonen and J. Engel, Phys. Rev. C **93**, 014304 (2016).

[20] J. T. Suhonen, Front. Phys. **5**, 55 (2017).

[21] A. Ravlić, E. Yüksel, Y. F. Niu, and N. Paar, Phys. Rev. C **104**, 054318 (2021).

[22] K. Langanke and G. Martínez-Pinedo, Rev. Mod. Phys. **75**, 819 (2003).

[23] E. Caurier, G. Martínez-Pinedo, F. Nowack, A. Poves, and A. P. Zuker, Rev. Mod. Phys. **77**, 427 (2005).

[24] S. Yoshida, Y. Utsuno, N. Shimizu, and T. Otsuka, Phys. Rev. C **97**, 054321 (2018).

[25] T. Suzuki, S. Shibagaki, T. Yoshida, T. Kajino, and T. Otsuka, Astrophys. J. **859**, 133 (2018).

[26] F. T. Avignone, S. R. Elliott, and J. Engel, Rev. Mod. Phys. **80**, 481 (2008).

[27] T. Nikšić, P. Marević, and D. Vretenar, Phys. Rev. C **89**, 044325 (2014).

[28] K. Kaneko, T. Mizusaki, Y. Sun, and S. Tazaki, Phys. Rev. C **92**, 044331 (2015).

[29] Z. H. Wang, J. Xiang, W. H. Long, and Z. P. Li, J. Phys. G: Nucl. Part. Phys. **42**, 045108 (2015).

[30] K. Nomura, R. Rodríguez-Guzmán, and L. M. Robledo, Phys. Rev. C **95**, 064310 (2017).

[31] R. Budaca, P. Buganu, and A. Budaca, Nucl. Phys. A **990**, 137 (2019).

[32] Nihad J. Aabu Awwad, H. Abusara, and S. Ahmad, Phys. Rev. C **101**, 064322 (2020).

[33] Y. Toh, C. J. Chiara, E. A. McCutchan, W. B. Walters, R. V. F. Janssens, M. P. Carpenter, S. Zhu, R. Broda, B. Fornal, B. P. Kay, F. G. Kondev, W. Królas, T. Lauritsen, C. J. Lister, T. Pawłat, D. Seweryniak, I. Stefanescu, N. J. Stone, J. Wrzesiński, K. Higashiyama *et al.*, Phys. Rev. C **87**, 041304(R) (2013).

[34] A. Corsi, J.-P. Delaroche, A. Obertelli, T. Baugher, D. Bazin, S. Boissinot, F. Flavigny, A. Gade, M. Girod, T. Glasmacher, G. F. Grinyer, W. Korten, J. Libert, J. Ljungvall, S. McDaniel, A. Ratkiewicz, A. Signoracci, R. Stroberg, B. Sulignano, and D. Weisshaar, Phys. Rev. C **88**, 044311 (2013).

[35] A. Ayangeakaa, R. Janssens, C. Wu, J. Allmond, J. Wood, S. Zhu, M. Albers, S. Almaraz-Calderon, B. Bucher, M. Carpenter, C. Chiara, D. Cline, H. Crawford, H. David, J. Harker, A. Hayes, C. Hoffman, B. Kay, K. Kolos, A. Korichi *et al.*, Phys. Lett. B **754**, 254 (2016).

[36] A. M. Forney, W. B. Walters, C. J. Chiara, R. V. F. Janssens, A. D. Ayangeakaa, J. Sethi, J. Harker, M. Alcorta, M. P. Carpenter, G. Gürdal, C. R. Hoffman, B. P. Kay, F. G. Kondev, T. Lauritsen, C. J. Lister, E. A. McCutchan, A. M. Rogers, D. Seweryniak, I. Stefanescu, and S. Zhu, Phys. Rev. Lett. **120**, 212501 (2018).

[37] M. Matejska-Minda, P. Bednarczyk, B. Fornal, F. R. Xu, W. Y. Liang, G. de Angelis, S. Aydin, S. Brambilla, M. Ciemała, E. Farnea, T. Hüyük, G. Jaworski, M. Kmiecik, M. Krzysiek, S. Leoni, A. Maj, R. Menegazzo, W. Meczynski, C. Michelagnoli, M. Palacz *et al.*, Phys. Rev. C **100**, 054330 (2019).

[38] S. Sekal, L. M. Fraile, R. Lică, M. J. G. Borge, W. B. Walters, A. Aprahamian, C. Benchouk, C. Bernards, J. A. Briz, B. Bucher, C. J. Chiara, Z. Dlouhý, I. Gheorghe, D. G. Ghiţă, P. Hoff, J. Jolie, U. Köster, W. Kurcewicz, H. Mach, N. Mărginean *et al.*, Phys. Rev. C **104**, 024317 (2021).

[39] K. Heyde and J. L. Wood, Rev. Mod. Phys. **83**, 1467 (2011).
[40] P. Ring and P. Schuck, *The Nuclear Many-Body Problem* (Springer, Berlin, 1980).
[41] K. Nomura, N. Shimizu, and T. Otsuka, Phys. Rev. Lett. **101**, 142501 (2008).
[42] F. Iachello and O. Scholten, Phys. Rev. Lett. **43**, 679 (1979).
[43] F. Iachello and P. Van Isacker, *The Interacting Boson-Fermion Model* (Cambridge University Press, Cambridge, 1991).
[44] S. Brant, V. Paar, and D. Vretenar, Z. Phys. A **319**, 355 (1984).
[45] L. M. Robledo, T. R. Rodríguez, and R. R. Rodríguez-Guzmán, J. Phys. G: Nucl. Part. Phys. **46**, 013001 (2019).
[46] D. Vretenar, A. V. Afanasjev, G. A. Lalazissis, and P. Ring, Phys. Rep. **409**, 101 (2005).
[47] T. Nikšić, D. Vretenar, and P. Ring, Prog. Part. Nucl. Phys. **66**, 519 (2011).
[48] T. Nikšić, N. Paar, D. Vretenar, and P. Ring, Comput. Phys. Commun. **185**, 1808 (2014).
[49] T. Nikšić, D. Vretenar, and P. Ring, Phys. Rev. C **78**, 034318 (2008).
[50] Y. Tian, Z. Y. Ma, and P. Ring, Phys. Lett. B **676**, 44 (2009).
[51] A. Bohr and B. R. Mottelson, *Nuclear Structure* (Benjamin, New York, 1975).
[52] T. Otsuka, A. Arima, and F. Iachello, Nucl. Phys. A **309**, 1 (1978).
[53] T. Otsuka, A. Arima, F. Iachello, and I. Talmi, Phys. Lett. B **76**, 139 (1978).
[54] O. Scholten, Prog. Part. Nucl. Phys. **14**, 189 (1985).
[55] S. Brant and V. Paar, Z. Phys. A **329**, 151 (1988).
[56] A. E. L. Dieperink, O. Scholten, and F. Iachello, Phys. Rev. Lett. **44**, 1747 (1980).
[57] J. N. Ginocchio and M. W. Kirson, Nucl. Phys. A **350**, 31 (1980).
[58] K. Nomura, N. Shimizu, and T. Otsuka, Phys. Rev. C **81**, 044307 (2010).
[59] K. Nomura, T. Otsuka, N. Shimizu, and L. Guo, Phys. Rev. C **83**, 041302(R) (2011).
[60] D. R. Inglis, Phys. Rev. **103**, 1786 (1956).
[61] S. T. Beliaev, Nucl. Phys. **24**, 322 (1961).
[62] K. Nomura, R. Rodríguez-Guzmán, and L. M. Robledo, Phys. Rev. C **101**, 014306 (2020).
[63] F. Dellagiacoma, Beta decay of odd mass nuclei in the interacting boson-fermion model, Ph.D. thesis, Yale University, 1988.
[64] G. A. Lalazissis, T. Nikšić, D. Vretenar, and P. Ring, Phys. Rev. C **71**, 024312 (2005).
[65] S. Goriely, S. Hilaire, M. Girod, and S. Péru, Phys. Rev. Lett. **102**, 242501 (2009).
[66] A. Frank, P. Van Isacker, and C. E. Vargas, Phys. Rev. C **69**, 034323 (2004).
[67] Brookhaven National Nuclear Data Center, http://www.nndc.bnl.gov.
[68] P. D. Duval and B. R. Barrett, Phys. Lett. B **100**, 223 (1981).
[69] P. Duval, D. Goutte, and M. Vergnes, Phys. Lett. B **124**, 297 (1983).
[70] K. Nomura, R. Rodríguez-Guzmán, L. M. Robledo, and N. Shimizu, Phys. Rev. C **86**, 034322 (2012).
[71] K. Nomura, T. Otsuka, and P. Van Isacker, J. Phys. G: Nucl. Part. Phys. **43**, 024008 (2016).
[72] K. Nomura, R. Rodríguez-Guzmán, and L. M. Robledo, Phys. Rev. C **94**, 044314 (2016).
[73] K. Nomura and J. Jolie, Phys. Rev. C **98**, 024303 (2018).
[74] N. Stone, At. Data Nucl. Data Tables **90**, 75 (2005).